Effect of Blowing Ratio on the Nusselt Number and Film Cooling Effectiveness Distributions of a Showerhead Film Cooled Blade in a Transonic Cascade

Ashley R. Guy

Thesis submitted to the faculty of the
Virginia Polytechnic Institute and State University
in partial fulfillment of the requirements for the degree of

Master's of Science
in
Mechanical Engineering

Dr. Wing Ng, Chair
Dr. Thomas Diller
Dr. Brian Vick

July 16, 2007
Blacksburg, Virginia

Keywords: Film Cooling,
Turbine Blade, Heat Transfer, Cascade

Effect of Blowing Ratio on the Nusselt Number and Film Cooling Effectiveness Distributions of a Showerhead Film Cooled Blade in a Transonic Cascade

Ashley R. Guy
Virginia Polytechnic Institute and State University, 2007
Advisor: Dr. Wing F. Ng

Thesis Abstract

To increase the efficiency of gas turbine engines, higher turbine operating temperatures have been employed. In order to keep the turbine component temperatures below their melting point, air from the compressor section of the turbine is ejected over the surface of the blade to provide a protective shroud of cooler air over the surface of the blades. Film cooling performance is difficult to predict analytically or computationally—for this reason, experiments are needed to properly characterize the performance of designed cooling schemes.

In this study, a first stage turbine blade with three rows of showerhead cooling holes was instrumented with heat flux gages to experimentally characterize the Nusselt Number and film cooling effectiveness distributions over the surface of the blade. The blade was arranged in a two-dimensional, linear cascade in a transonic, blowdown-type wind tunnel. The wind tunnel freestream conditions were varied over two exit Mach numbers, M_e=0.78 and M_e=1.01, with an inlet freestream turbulence intensity of 12% with an integral length scale normalized by blade chord of 0.26 generated by a passive mesh turbulence grid. The coolant conditions were varied by changing the ratio of coolant to freestream mass flux, blowing ratio, over three values: BR=0.60, 1.0, and 1.5.

Film cooling performance is characterized by experimental results in terms of Nusselt number and film cooling effectiveness distributions. These distributions are the result of five measurement locations over an extent of s/d=-32 on the pressure side to s/d=33 on the suction side. Film cooling was found to increase Nusselt number over the entire measurement domain, and increasing the blowing ratio also increased the Nusselt number. Of the blowing ratios tested, a blowing ratio of 1.0 was found to have superior heat load reduction performance at both freestream conditions tested.

Acknowledgements

This study was sponsored by Solar Turbines and conducted under the direction of Drs. Hee-Koo Moon and Luzeng Zhang. I would like to thank them for their support and guidance over the duration of this project. I would also like to thank Drs. Mark Polanka and Richard Anthony of the Air Force Research Laboratory for the manufacture of the thin film gages that were critical to this project. Thanks to the Aerojet corporation for providing funding for my fellowship and their continued support of Virginia Tech Mechanical Engineering.

The members of my committee have been invaluable to the success of this project. Starting with his teaching, and continuing through the opportunities he has given me to work on many research projects during the past several years, Dr. Ng has been a great mentor over the course of my academic career. He is a truly wonderful manager that gives a great deal of trust and responsibility to his students. Without Dr. Diller's advice and judgment, this project could not have proven a success. His experience was always there for the team at critical junctions of this project because of the generosity with which he gives his time. Dr. Vick is an unparalleled teacher. One of the most important attitudes I will take away from Virginia Tech comes from Dr. Vick's teaching philosophy-make sure your understand the fundamentals in detail.

My research team has been the most valuable part of my work. This project was truly a team effort, and without Shakeel Nassir, Trey Bolchoz, and Jeff Carullo I would simply not be graduating. Words cannot express my gratitude. I would also like to thank the M.E. office and shop for all of their help. Bill Songer has proved and invaluable part of all the projects I have taken part in, and both his work and humor have gotten me through.

I would like to thank my family and friends. My family has given me everything that I could ever expect and more. There is no way to thank your family the way they deserve, but I hope that this thesis and degree will help to show that a bit of their hard work has paid off. To my friends that have become my extended family, I cannot say enough.

My parents, Bill and Raye Guy, grandma, Barbara Shiley, and aunt, Evelene Curry, made it possible for my sister, Margaret, and I to attend Virginia Tech. Nowhere on earth would have suited me better and I am grateful for the opportunity.

I would also like to extend my gratitude to the Virginia Tech community. The strength, sensitivity, and fortitude that has been shown is something we can all be proud of. Anyone who has experienced this community could have told you that we have something special--even before the tragic events of this past April. While we all share a deep sense of sorrow, I think we can be proud that we have shown what it means to be Virginia Tech.

Attribution

This research project was the result of a team effort, and the paper that forms the body of this thesis is coauthored by the members of this research team. Included in the "Attribution" section is a description of the author's contribution to this work.

Shakeel Nasir- M.S.M.E. (Department of Mechanical Engineering), Virginia Tech is a Ph.D. candidate in mechanical engineering and a member of the author's research team that undertook this project. Shakeel assisted with the design of experiment, manufacturing of test articles, installation, data reduction, and with the review of literature as part of the requirements of his studies.

Ruford Bolchoz- B.S.M.E. (Department of Mechanical Engineering), Virginia Tech is a master's candidate in mechanical engineering and a member of the author's research team that undertook this project. Ruford built the film cooling circuit that was used in this project and authored the checklists provided in Appendix A. He also helped with running the experiment and data reduction.

Prof. Wing F. Ng- Ph.D. (Department of Mechanical Engineering), Virginia Tech is the primary Advisor and Committee Chair. His leadership and advice guided the team throughout this work.

Luzeng Zhang- Ph.D. (Senior Principal Engineer, Heat Transfer), Solar Turbines Inc.
Hee K. Moon- Ph.D. (Group Manager, Heat Transfer), Solar Turbines Inc. Drs. Zhang and Moon provided the design of the film cooled blade that was used in this testing. They also helped the team by discussing the "three temperature problem" associated with film cooling research. Solar Turbines Inc. provided the funding for this work.

Table of Contents

List of Figures

List of Tables

Preface

In the drive to increase the efficiency of gas turbine engines, higher operating temperatures have been employed by engine designers. The operating temperature can be above engine component melting points. A method used to protect components is film cooling. Turbine blades are equipped with a plenum and an array of cooling holes. Cooler air from the compressor section of the engine is ejected over the blade surface forming a shroud of air that protects the engine components from the hot gas exiting the combustor.

Because this process involves the mixing of gases at different speeds, densities, temperatures, and flow directions at high freestream turbulence, it has been challenging to model analytically or to predict with current CFD methods. Experimental studies are necessary to provide engineers with the adequate parameters needed to predict the performance and lifespan of the components they design.

The study of film cooling is inherently a study in design balance. When considering cooling system design on an engine scale, increasing the amount of coolant supplied yields a cooler blade that will last longer, but decreases engine core flow--diminishing efficiency. Interestingly, when contemplating the physics of film cooling, balance is also the key to developing an effective design. Increasing the amount of coolant injected reduces the driving temperature of heat transfer, but more coolant augments boundary layer disturbance--providing a higher heat transfer coefficient. So, if the designer does not balance the decrease in driving potential with the increase in heat transfer coefficient, he or she will not decrease the heat load experienced by the engine component.

This thesis, on a fundamental level, explores the aspects of film cooling balance by measuring film cooling performance at different rates of coolant injection at varying freestream flow conditions. The driving temperature of heat transfer is presented in terms of film cooling effectiveness and the heat transfer coefficient is provided as the Nusselt number. The effect of the amount of coolant supplied is studied by varying the blowing ratio. The effect of the freestream is examined by measuring film cooling performance at two Mach numbers. This thesis is arranged in a conference paper format with subsequent appendices attached to expand and support ideas presented in the paper.

Effect of Blowing Ratio on the Nusselt Number and Film Cooling Effectiveness Distributions of a Showerhead Film Cooled Blade in a Transonic Cascade

A. R. Guy, S. Nasir, R. Bolchoz, and W.F. Ng
Mechanical Engineering Department
Virginia Polytechnic Institute and State University
Blacksburg, VA 24061

L.J. Zhang and H.K. Moon
Solar Turbines Inc.
San Diego, CA 92101

Abstract

This paper investigates the effect of blowing ratio on the film cooling performance of a showerhead film cooled first stage turbine blade. The blade was instrumented with double-sided thin film heat flux gages to experimentally characterize the Nusselt number and film cooling effectiveness distributions over the surface of the blade. The blade was arranged in a two-dimensional, linear cascade within a transonic, blowdown type wind tunnel. The wind tunnel freestream conditions were varied over two exit Mach numbers, M_e=0.78 and M_e=1.01, with an inlet freestream turbulence intensity of 12% , with an integral length scale normalized by blade chord of 0.26 generated by a passive, mesh turbulence grid. The coolant conditions were varied by changing the ratio of coolant to freestream mass flux, blowing ratio, over three values, BR=0.60, 1.0, and 1.5 while keeping a density ratio of 1.7.

Experimental results show that ingestion of freestream flow into the showerhead cooling plenum can occur below a blowing ratio of 0.6. Film cooling increases Nusselt number over the uncooled case and increasing the blowing ratio also increases Nusselt number. At a blowing ratio of 1.5 and M_e=1.01 a large drop in effectiveness just downstream of injection on both the pressure and suction surfaces is evidence of jet liftoff. The blowing ratio of 1.0 was found to have superior heat load reduction over the blade surface at both freestream conditions tested. The blowing ratio of 1.0 reduced the heat load by as much as 39% and 32% at M_e=0.78 and 1.01, respectively.

Nomenclature

A	area
BR	blowing ratio
C	blade true chord
d	cooling hole diameter
DR	density ratio
h	heat transfer coefficient
k	conductivity
l	thickness of gage
LS	integral length scale
M	Mach Number
$\dot{m}$	mass flow rate
Nu	Nusselt Number
P	blade pitch
p	cooling hole pitch
PS	pressure side
q''	heat flux
r	turbulent recovery factor
Re	Reynolds Number
s	surface distance
SS	suction side
T	temperature
Tu	freestream turbulence intensity in the streamwise direction
U	velocity

Greek

ϕ	overall film cooling effectiveness
α	spanwise cooling hole angle
γ	specific heat ratio
η	film cooling effectiveness
ρ	density

Subscripts

0	total
∞	freestream
aw	adiabatic wall temperature
b	backwall thermocouple
c	coolant
e	exit
f	film cooling
i	inlet
loc	local
o	no film cooling
r	recovery
red	reduction
w	wall, Pt TFG surface

Introduction

In the drive to increase the efficiency of gas turbine engines, higher and higher engine operating temperatures have been employed by engine manufacturers. These temperatures can become so high that they are above the melting temperature engine components themselves. A method used to protect the components from melting is film cooling. In this method, turbine blades are equipped with a plenum and an array of cooling holes arranged over their surface. Cooler air from the compressor section of the engine is blown through these holes where it forms a thin film of cool air separating the engine components from the hot gas path. The cooling air protects the blade from the extreme temperatures of the gases that have just left the combustion portion of the engine.

Because this process involves the mixing of gases at different speeds, densities, temperatures, and flow directions, it has been extremely challenging to model analytically or to predict with current CFD methods. For this reason, experimental studies are necessary to provide engineers with the adequate parameters to predict the performance and lifespan of the components they design.

The current study presents experimental results examining the effect of blowing ratio on the film cooling performance of a showerhead film cooled turbine blade at different Mach numbers. The performance of film cooling has been characterized by measuring the Nusselt number and film cooling effectiveness distribution over the surface of a showerhead film cooled blade.

Summary of Literature

Film Cooling is a broad, mature topic and its varied applications have been studied in the literature for some time. The basic film cooling physics are described by Goldstein [1]. Bogard and Thole [2] and Han *et al.* [3] have compiled much of the current work on film cooling as it applies to the gas turbine field. The current experimental work concerns a turbine blade in a high speed environment. Therefore, the literature review has been limited to airfoils in both low and high speed environments. Literature is presented in increasing relevance beginning with low speed vane and blade studies and concluding with high speed vane and blade experiments.

Low Speed Vane. Ames [4] studied the effects of turbulence and rate of coolant injection on a film cooled C3X vane in a low speed facility at two Reynolds numbers. Several film cooling geometries were studied, but the showerhead cooled vane results are of interest to this study. Ames used thermocouples to measure the surface temperature distribution with foil heaters supplying heat flux and a finite element analysis to correct for two-dimensional internal conduction. The results showed that film cooling augmented Stanton number in the both the laminar and turbulent regions of the vane with more augmentation in the laminar region. Increasing the rate of coolant injection increased the levels of Stanton number augmentation. The effect of coolant injection rate on effectiveness was shown to be greater than the effect of Reynolds number on effectiveness. The effect of freestream turbulence was observed to reduce the levels of film cooling effectiveness and also quicken the dissipation of cooling effectiveness.

Low Speed Blade. A study of coolant density ratio and the impact of an upstream wake were studied in a low speed linear fully film cooled blade cascade by Ou *et al.*[5] and Mehendale *et al.*[6]. Heat transfer coefficient is reported by [6], while effectiveness and heat load reduction are presented by [7]. Density ratio was varied by using air and CO_2 as the two coolant gases and a spoked wheel wake generator simulated blades passing an upstream wake. Film cooling increased the heat transfer coefficient over the surface of the blade and it was found that cooling injection had a more dominant effect on heat transfer coefficient than the addition of the upstream wake. An increase in the mass flux ratio, blowing ratio, was seen to increase heat transfer coefficient. The addition of the wake reduced film cooling effectiveness. Different blowing ratios were seen to provide the highest effectiveness levels for air and CO_2 injection. However, it was noted that reported values of effectiveness for the higher density, CO_2, case could be conservative due to the specific heat differences between air and CO_2. The best blowing ratio in the range of 0.4-1.2 studied, in terms of heat load reduction, was determined to be 0.8 and 1.2 for air and CO_2, respectively. The addition of grid turbulence on film cooling performance was studied in the same facility by Ekkad *et al.*[6]. Superimposing turbulence from a grid on a wake was found to increase heat transfer coefficients and decrease film cooling effectiveness. However, at a high enough level of freestream

turbulence, the unsteady wake was shown to have negligible effect on film cooling performance.

High Speed Vane. The effects of varying Reynolds number, Mach number, coolant injection rate, and coolant to temperature ratio were studied on a showerhead cooled C3X vane in a transonic, linear cascade by Turner *et al.* [8]. Increasing the rate of coolant injection was seen to increase the heat transfer coefficient. Increases in Reynolds number in the film cooled case were also seen to augment the film cooled heat transfer coefficient. It was noted that the addition of film cooling had a definite effect on heat transfer coefficient in the laminar region, but after transition the effect of film cooling was negligible. While not dramatically, film cooling was shown to move the location of laminar to turbulent transition farther upstream.

Drost and Bölcs [9] studied the effect of varying Mach number, density ratio, blowing ratio, and freestream turbulence on a high speed vane. The transient liquid crystal technique was used to determine h and η. An increase in effectiveness was observed with an increase in blowing ratio. For a double row of film cooling holes on the suction surface, between blowing ratios of 1.11 and 1.77 jet liftoff was observed. For increasing blowing ratio, increasing heat transfer coefficient augmentation was also observed. On the suction side, the reduction of heat load is higher closer to injection for lower blowing ratios and higher farther downstream of injection for higher blowing ratios. For the pressure side, a heat load increase was seen for blowing ratios above 1.3.

Guo *et al.* [10] used platinum thin film gages on a semi-infinite substrate in a transonic annular cascade to measure the effect of film cooling on a fully cooled nozzle guide vane. Foreign gas with specific heat properties similar to air was used to match the density ratio seen in a gas turbine. Augmentation of heat transfer coefficient due to cooling was observed over the entire pressure surface and some of the suction surface. Heat transfer coefficient levels below that of uncooled data are reasoned to be the result of a thicker boundary layer. Effectiveness was higher on the pressure side where more rows of coolant injection were present and decreased after the last row of cooling holes. Piccini *et al.* [11] developed a type of double-sided thin film gage by adding a thermocouple beneath the thin film gages used by [10]. A variation of this type of double-sided gage is used in this work.

High Speed Blade. Camci and Arts [12] measured heat transfer coefficient over a film cooled blade in a short duration, high speed facility with thin film gages mounted on a semi-infinite, Macor blade. The effect of internal conduction in the blade plenum region was accounted for by reporting a higher uncertainty closer to the plenum region. Increasing the coolant mass flow was observed to decrease the heat transfer coefficient and cooled heat transfer coefficient levels were observed below the levels of an uncooled case.

Rigby *et al.* [13] tested a range of film cooling geometries, blowing ratios, and the effect of upstream passing shocks and wakes on the film cooling performance in a two dimensional linear cascade. On the suction surface, increasing the blowing ratio was noted to decrease heat transfer coefficient below the uncooled case. Also on the suction surface, film coolant liftoff was assumed because of a drop of effectiveness between a blowing ratio of 1.0 and 1.5. Schlieren photography captured this coolant liftoff. Shock and bar passing were seen to decrease film cooling effectiveness.

The geometry studied by [13] was tested in MIT's blowdown turbine test facility in a full rotating stage by Abhari and Epstein[14]. Tests included the effect of upstream wake passing and upstream NGV trailing edge blowing. Hub, tip, and midspan of the blade were instrumented with thin film gages and time averaged and time resolved data are presented. A reduction in heat transfer coefficient was said to take place with the introduction of film cooling in both the time averaged and time resolved data. Of the two blowing ratios studied, the higher blowing ratio provided less effective cooling than the lower blowing ratio.

References [12], [13], and [14] report a decrease in heat transfer coefficient for the addition of film cooling because these experimental approaches do not define the heat transfer coefficient in terms of the adiabatic wall temperature. In these cases, a decrease in the heat transfer coefficient is interpreted as a decrease of heat flux due to film cooling.

Film cooling was studied on a highly turned blade in the linear, transonic, long-duration, Virginia Tech, wind tunnel by Smith *et al.* [15]. Heat transfer coefficient measurements were made on the suction side of a showerhead cooled blade with additional pressure side and suction side gill cooling hole rows. Heat transfer coefficient was seen to increase with the addition of film cooling. The film coolant supplied was air

that was cooled to provide an engine realistic density ratio. Plenum to freestream pressure ratio was varied to study the effect of varying coolant injection.

Effectiveness measurements were completed by Zhang and Moon [16] on a showerhead film cooled turbine blade designed by Solar Turbines using the pressure sensitive paint technique. The effectiveness of several cooling geometries was investigated. A showerhead cooling scheme with three rows of cylindrical holes was shown to provide the most two-dimensional spanwise distribution of effectiveness. The effect of turbulence and Reynolds number on the heat transfer coefficient distribution of an uncooled version of the blade geometry used by [16] was completed by Carullo *et al.* [17]. The current study presents the heat transfer coefficient distribution, film cooling effectiveness, and net heat flux reduction of the cooled blade geometry described by [16] and compared to the uncooled measurements of [17]. The heat transfer distribution is studied over a range of Mach numbers and coolant injection rates in a linear, transonic environment with an engine representative coolant to freestream density ratio.

Experimental Apparatus

The following section is arranged into several different parts. The "Wind Tunnel Facility" section describes how the freestream flow conditions were imposed on the test blade. The "Showerhead Film Cooled Blade" section describes the blade testing and its cooling geometry. The "Film Cooling" section describes the cooling parameters and the measurement of heat flux is described in "Double-sided Heat Flux Gage".

Wind Tunnel Facility

Testing was performed in the transonic cascade wind tunnel at Virginia Tech. A schematic is shown in Figure 1. The facility is a long-duration blowdown type wind tunnel capable of achieving a steady Mach number for up to 20 seconds. Air is compressed, dried, and stored in external tanks. When the tunnel is started, air passes through a valve that keeps the test condition constant. The air then proceeds through a bank of heated copper tubes that act as a passive heat exchanger and as flow straighteners. Freestream turbulence is generated by a passive, mesh grid. All testing was done at a turbulence intensity of 12% with an integral length scale normalized by

blade pitch of 0.26 Carullo *et al.* [17]. This turbulence measurement was made by a traversing hot wire probe 0.6C upstream of the blade leading edge. The turbulence grid geometry and measurements of turbulence are described further by Carullo *et al.* [17]. Air reaches the test section at a steady Mach number and a transient, decreasing total temperature.

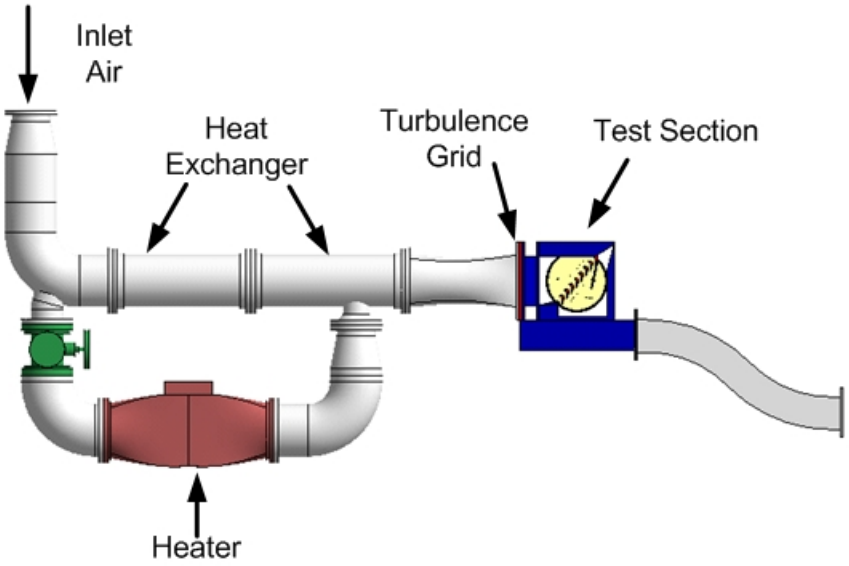

Figure 1. Transonic cascade wind tunnel. Carullo *et al.* [17]

Showerhead Film Cooled Blade

A showerhead film cooled blade with three rows of cylindrical cooling holes was used in this study. The blade is a 2x scaled version of a 1st stage turbine blade geometry provided by Solar Turbines. The film cooled blade was the middle blade in a linear cascade of seven full blades and two half blades. It was the only blade in the cascade outfitted for film cooling and heat transfer measurements. The cascade geometry is further described by Carullo[18]. Table 1 provides the details of the blade and cooling geometry and a profile of the blade is shown in Figure 2.

Table 1. Showerhead cooled blade geometry

True Chord	*C*	69.9 mm (2.75 in.)
Pitch	*P*	58.2 mm (2.29 in.)
Cooling Hole Diameter	*d*	0.838 mm (0.033 in.)
Spanwise Angle	*α*	30º
Cooling Hole Spacing	*p/d*	6
Blade Span		152.4 mm (6.00 in.)
Cooled Span		76.2 mm (3.00 in.)
Turning Angle		107.5°

The exit of the center row of cooling holes is placed at the geometric stagnation point on the blade. The pressure and suction side rows of film cooling holes are spaced at equal distances from the stagnation. There are 15 cooling holes in the stagnation row and 16 holes in the pressure and suction side rows. The cooling rows are staggered to provide for more even coverage of coolant. The stagnation row is arranged on the test blade with the center hole of the row at midspan while the pressure and suction side rows are arranged so that their cooling hole pattern starts halfway between the spacing of stagnation row holes. Cooling flow is injected at 30º angle to the span of the blade as shown in Figure 3. All cooling hole rows have the same spanwise injection angle.

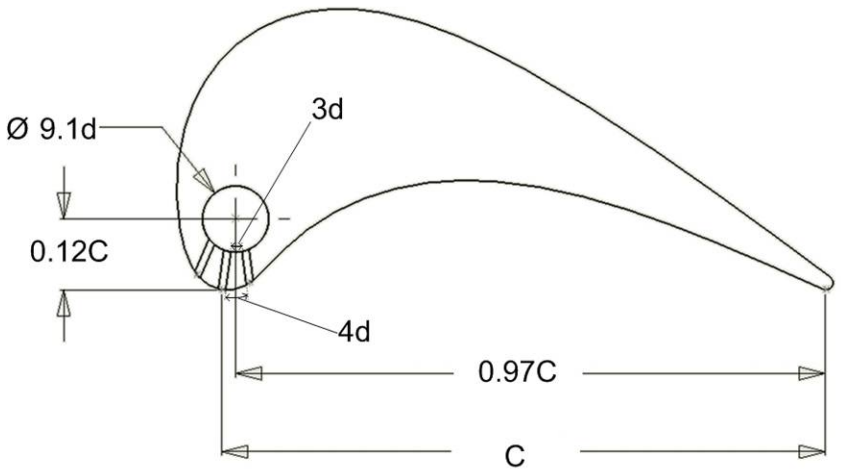

Figure 2. Profile view of showerhead film cooled blade

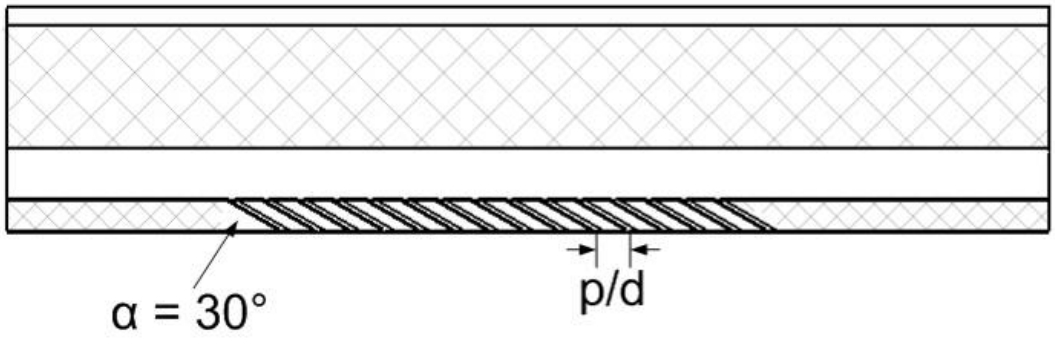

Figure 3. Section view of showerhead film cooled blade. Section through the stagnation row of holes.

Film Cooling

The film cooling parameters explored in this study were picked in an attempt to match those used in a gas turbine engine. Coolant was supplied to the blade from a storage tank pressurized with filtered, dried air to 120 psi. The air was dried to a relative humidity less than 4%. The air exited the tank was regulated by a pneumatic control valve and passed through a coil of pipe immersed in liquid nitrogen. The amount of liquid nitrogen was manipulated to provide a coolant to freestream density ratio, *DR*, defined as

$$DR = \frac{\rho_c}{\rho_\infty} \tag{1}$$

The freestream density was calculated from cascade inlet conditions measured by a pitot-static probe and a T-type thermocouple. The coolant density was determined from a T-type thermocouple inserted near midspan at the center of the blade plenum and a pitot-static probe near at the entrance to the plenum. The density ratio was kept at DR~1.7 for all of the tested conditions. This density ratio is near that employed in a gas turbine Bogard and Thole [2].

The coolant to freestream mass flux ratio, blowing ratio, is

$$BR = \frac{\rho_c U_c}{\rho_\infty U_\infty} = \frac{\dot{m}_c}{A_{holes}\rho_i U_i} \tag{2}$$

where the mass flow into the plenum was measured with an orifice plate meter and divided by the area of the film cooling holes to find the coolant mass flux. The freestream mass flux was calculated from inlet flow conditions. The blowing ratio is calculated for the entire showerhead region using the definition outlined by Colban *et al.*[19]. Because local pressure variations at each of the cooling row locations, the blowing ratio will vary from row to row, but this variation is small. The blowing ratio was varied over three test conditions, BR=0.6, 1.0, and 1.5, by manipulating the pneumatic control valve to increase or decrease the supply of coolant. Blowing ratio uncertainty was determined to ±1.4% and density ratio ±0.4%.

Double-sided Heat Flux Gage

Previous work by Carullo *et al.* [17] with an uncooled blade, used single-sided platinum thin film gages to calculate heat flux based on a one dimensional heat flux, semi-infinite assumption. In this film cooling study, cold (-40º C) coolant injected into the plenum caused internal conduction within the blade's leading edge area during the tunnel run. This internal conduction phenomenon invalidated the one-dimensional heat flux assumption and necessitated the use of a double-sided gage for this study of film cooling performance.

Picccini *et al*. [11] used thermocouples mounted in an aluminum blade with overlaid platinum thin film gages. In the current research, this technique was adopted to construct a double-sided gage with a Platinum thin film gage, Pt TFG, overlaying a thin foil T-type thermocouple manufactured by RDF. The thinness of the thermocouple, 13 μm (0.5 mil), allowed it to be mounted to the adhesive backing of the Pt TFG and then applied to the blade. In the current work, the blade was manufactured from a low thermal conductivity glass, Macor. A diagram and photograph of the current gage is provided in Figure 4.

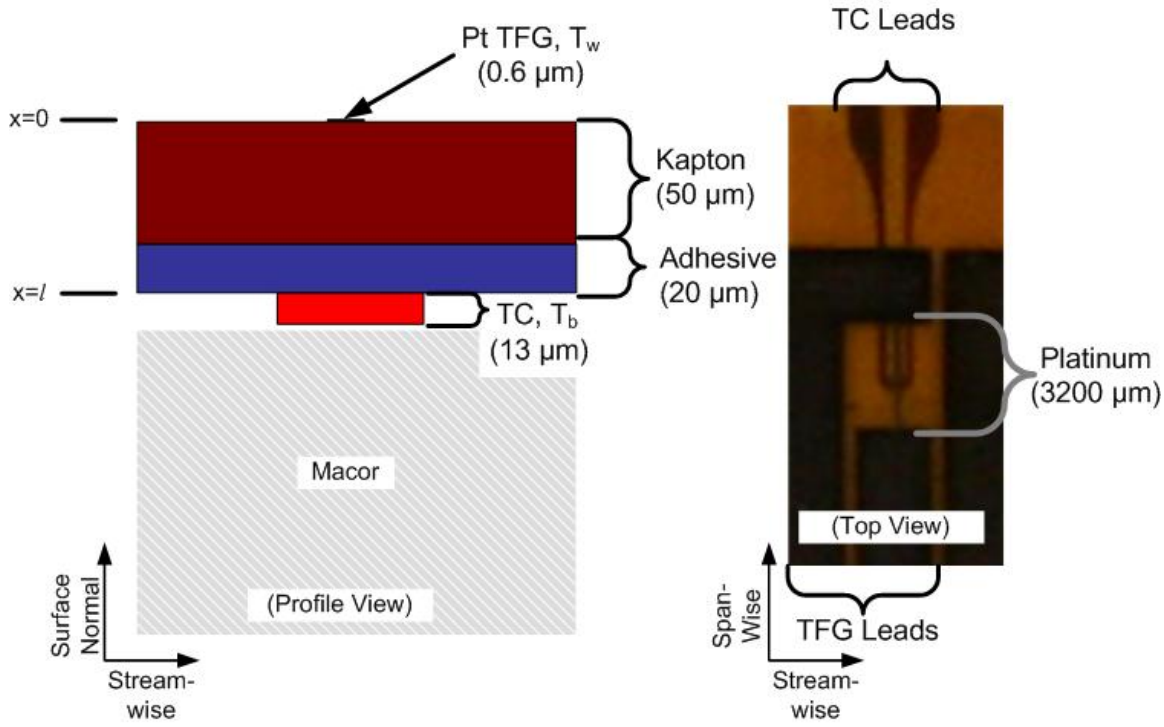

Figure 4. Double-sided Gage - (L) Profile Schematic of Gage (R) Top View of Gage.

The insulating material between the two temperature measurements is kapton. This material has a low thermal conductivity providing a large temperature difference across the gage thickness. The magnitude of this heat flux in the normal direction across the gage is several orders of magnitude greater than the heat flux in the longitudinal direction between gage mounting locations. This allows for the assumption of one-dimensional heat transfer across the gage. The low frequency heat flux can be calculated from

$$q'' = k/l\,(T_w - T_b) \tag{3}$$

The quantity *k/l* is the thermal conductivity divided by the thickness of the gage. Details regarding the determination of this quantity are provided in the "Material Properties Calibration" section. The Pt thin film gage is a resistance temperature device and is calibrated before its use in the facility. Details of this calibration and gage operation are found in Cress *et al*.[20].

Material Properties Calibration. The material properties of the kapton and adhesive layer of the gage were determined using an in-situ calibration technique.

During a tunnel run without film cooling, three gages located away from the plenum of the blade where the heat flux into the macor blade was one-dimensional and semi-infinite were selected. The backwall thermocouple was used as an input to a finite difference code developed by Cress[20] to solve for the heat flux into the blade. The heat flux from the finite difference code, thin film gage temperature, and backwall thermocouple temperature where used to solve Equation 3 for the value of *k/l*. For three gages over three tunnel runs the k/l value was determined to be 1240 ± 90 W/m^2-K using the 95% confidence interval. Bias error was found using Moffat's small perturbation method[21] and precision error was found from gage to gage and run to run repeatability. Assuming that the adhesive layer does not change its thickness due to mounting, the conductivity of the kapton used in the current research was found to be 0.09 ± 0.006 W/m-K.

Gage Mounting. To construct the double-sided gages, the adhesive backing on the thin film gages was exposed. The foil thermocouples' sensing area was aligned with the midspan of the platinum thin film gage sensing area. Thermocouples were placed beneath each thin film gage location and the leads of the thermocouple were extended along the opposite spanwise side of the blade as the platinum thin film gage copper leads. After the entire sheet of thin film gages was instrumented with thermocouples, the sheet was secured to the blade. Gages were mounted directly over the midspan of the blade with great care taken to avoid any air bubbles or gage to gage variation in mounting. The gage mounting is shown in Figure 5. The cooling holes were drilled in the gage sheet using the holes drilled in the blade as a guide. Thin film gages were wired and calibrated using the procedure outlined by Carullo [18]. Thermocouple wire was soldered to the leads of the foil thermocouples and secured within the data acquisition system.

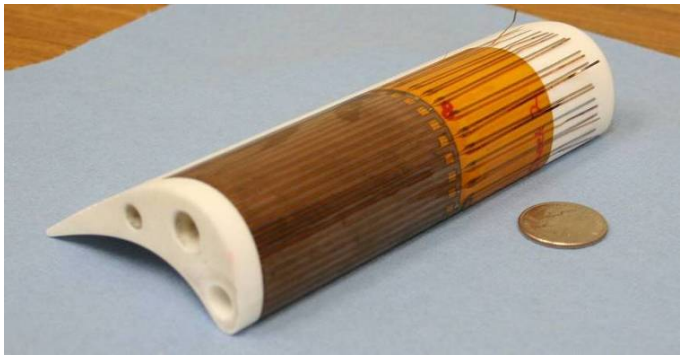

Figure 5. Gages installed to blade surface.

A total of 16 double-sided gages were mounted on the blade surface. The mounting of the thermocouple beneath the platinum gage sheet added complexities to the instrumentation package. These problems became evident as many gages were lost due to the sensitive nature of implementing a double-sided gage. The gages that were lost showed results that were unrepeatable or data that was not physical in nature and these gages were eliminated from analysis. Contact resistance between the thermocouple and blade, inherent installation inconsistencies, adhesion of the gage sheet, and difficulties with soldering and ruggedness of the platinum thin film gage are the probable causes of gage failure.

Five gages remained over a span of s/d=-32 on the pressure side to s/d=33 on the suction side of the blade. These gages provided results that were repeatable and trends that were in agreement with the literature. The results from these gages are reported in this paper and their locations are shown in Figure 6.

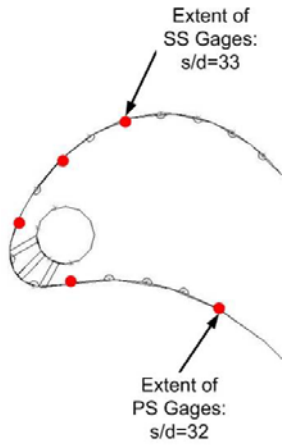

Figure 6. Extent of gages.

Calculation of Nusselt Number and Film Cooling Effectiveness

Heat transfer in a film cooled environment can be described by

$$q'' = h\left(T_{aw} - T_w\right) \tag{4}$$

where T_{aw} is the temperature of an assumed adiabatic wall that is the driving temperature of heat transfer. This adiabatic wall temperature is the temperature of the mixture of the freestream and injected fluid providing for heat transfer from the hot freestream into a blade wall that is protected by coolant Goldstein [1]. T_w was measured on the surface of

the blade using the platinum thin film gage. The adiabatic wall temperature can be nondimensionalized into the film cooling effectiveness

$$\eta = \frac{T_{aw} - T_r}{T_c - T_r} \tag{5}$$

where the recovery temperature of the freestream flow is determined by

$$T_r = T_{0,\infty}\left(\frac{1 + r\frac{\gamma - 1}{2}M_{loc}^{\ 2}}{1 + \frac{\gamma - 1}{2}M_{loc}^{\ 2}}\right) \tag{6}$$

where the local Mach number was determined from local static pressure tap measurements by Carullo *et al.*[17]. Because of coolant injection, the boundary layer was assumed to be turbulent everywhere downstream of injections. So, the recovery factor was determined by $r=Pr^{1/3}$.

In film cooling, h and η are the two quantities of interest. It is often necessary to determine these values from separate experiments. In the Virginia Tech facility, flow conditions are at quasi-steady state while the temperature of the freestream is transient. This allows for determination of heat transfer coefficient and film cooling effectiveness during a single tunnel run. This data analysis procedure is outlined in Smith *et al.*[15]. Equations 4 and 5 can be arranged to yield

$$\frac{q''}{T_r - T_c} = h\left(\frac{T_r - T_w}{T_r - T_c}\right) - h\eta \tag{7}$$

where *q"* is measured with the double-sided heat flux gage. In this form Equation 7 is equivalent to the standard line equation of y=mx+b. The coefficient multiplied by h in Equation 7 is plotted as the x-axis and the left side of the equation is plotted as the y-axis. An example of this plotting is shown in Figure 7.

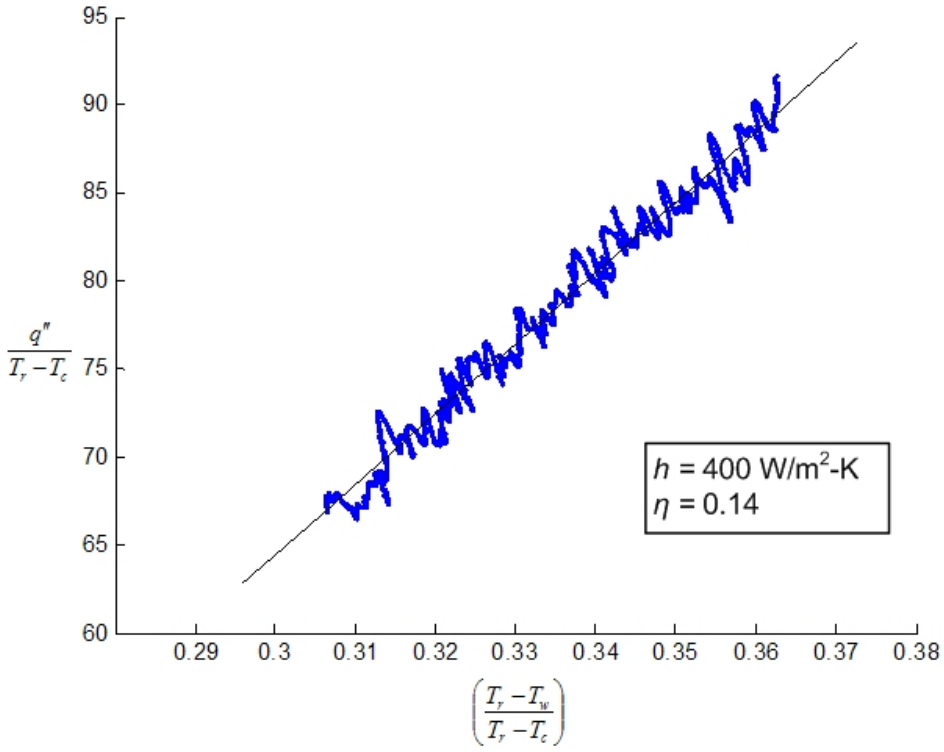

Figure 7. Determination of h and η

The slope of the line is the heat transfer coefficient and the x-intercept is the film cooling effectiveness. The slope is determined using a least squares linear regression fit of the plotted data. The effectiveness is given by the intersection of the x-axis—where *q"* goes to zero. The heat transfer coefficient and effectiveness were determined at each instrumented location for each tunnel run. The heat transfer coefficient results were nondimensionalized in terms of Nusselt number described by

$$Nu = \frac{hC}{k_\infty} \tag{8}$$

Experimental Uncertainty

The uncertainty of the quantities of interest, h and η, were determined with the aid of two methods. First, Moffat's [21] small perturbation uncertainty method was used to estimate the bias uncertainty of the x values and y values plotted in Figure 7. Brown *et al.*'s[22] method of determining linear curve fit uncertainty was used to obtain the uncertainty of the fit based upon the x and y uncertainty of each data point. All

uncertainties are reported as the 95% confidence interval. The uncertainty of the heat transfer coefficient was determined to be ±10%. Because η is determined from extrapolating the data shown in Figure 7, its uncertainty is larger. The uncertainty in η is ±20%.

Test Conditions

Two Mach numbers with three blowing ratios at each Mach number were investigated. In this study, the Mach and Reynolds number were coupled. Mach and Reynolds numbers are calculated based on exit conditions. Reynolds number is based on the blade true chord. The test conditions are provided in Table 2.

Table 2. Test Matrix

Freestream Condition	Blowing Ratio
M_e=0.78 (Re_e=800,000) (design condition)	0.6
	1.0
	1.5
M_e=1.01 (Re_e=1,100,000)	0.6
	1.0
	1.5

A sample of flow conditions and temperature are provided in Figure 8. In order to minimize the signal to noise ratio in the double-sided gage calculation of heat flux shown in Equation 3, the temperature difference across the gage should be high. For this reason, heat transfer data was reduced over a three second time window as soon as freestream flow conditions reached quasi-steady state. This time period corresponds to the highest tunnel to blade heat flux during quasi-steady flow conditions. Blowing ratios are transient over the course of data reduction, but this change is small and average values are reported in the description of results. In the sample data presented in Figure 8, blowing ratio decreases from a beginning value of 1.06 to 1.01 at the end of data reduction. Similarly density ratio changes from 1.70 to 1.66 over the course of the run. In Figure 7, it can be observed that the heat transfer coefficient is steady; so, the small

variability of density ratio and blowing ratio over the course of data reduction has a negligible impact on heat transfer coefficient.

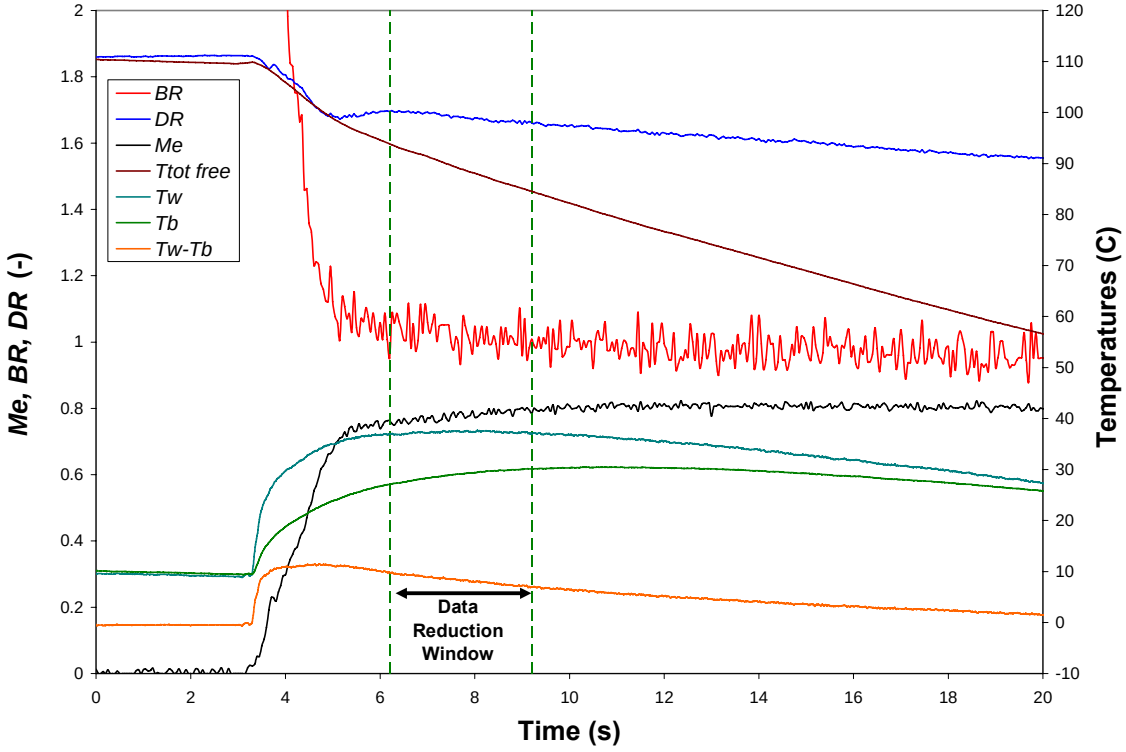

Figure 8. Sample Tunnel Run. Exit Mach number, blowing ratio, and density ratio are plotted on the left axis while temperatures are on the right axis.

Results

The "Results" section is divided into sections presenting *Nu* and η at each of the two Mach numbers presented. The effect of blowing ratio on *Nu* and η distributions are presented at the two Mach numbers tested. The effect of Mach number is explored by comparing the results of the same blowing ratio at the two freestream conditions tested. Nu_0 is defined as the Nusselt number determined for the blade without film cooling. These results were determined by Carullo *et al.* [17]. The effect of blowing ratio on net heat flux reduction at two Mach numbers are also presented.

Ingestion at *BR*=0.6

At the low blowing ratio case of *BR*=0.6, ingestion of freestream flow into the plenum was noticed. An example of this ingestion is provided in Figure 9. Just after the tunnel is started, ingestion into the plenum is indicated by an increase in plenum temperature. Throughout the run, ingestion can be noticed by fluctuation in plenum temperature not observed in the higher blowing ratio cases. Since there is a variation in the local freestream pressures between cooling hole rows, it is possible to be ingesting freestream flow at one cooling hole row, and still be ejecting coolant from the other rows. Ingestion of freestream flow in film cooling at high freestream speeds was noted by Smith *et al.*[23]. Since ingestion was noted at *BR*=0.6, results are not presented at this test condition.

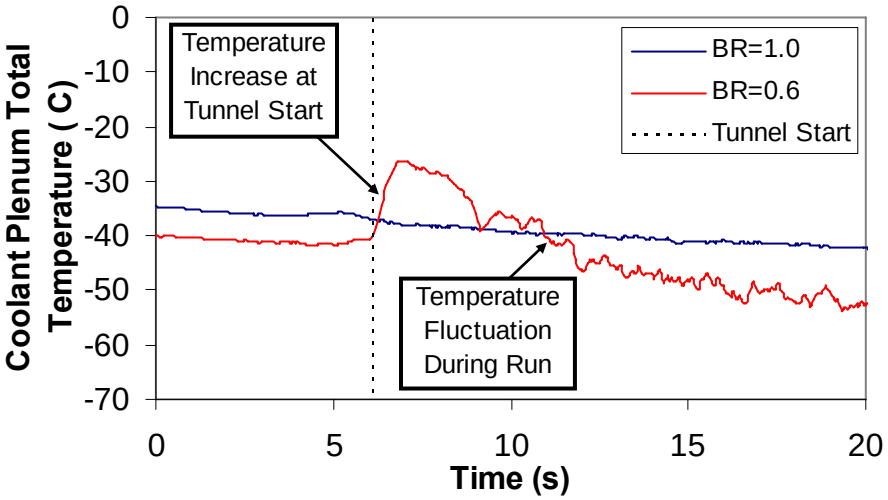

Figure 9. Freestream flow ingestion at *BR*=0.6 compared to a nominal run at *BR*=1.0.

Effect of Blowing Ratio at M_e=0.78

The effect of blowing ratio on heat transfer coefficient is provided in Figure 10 and the increase compared to an uncooled blade is provided in Figure 11. On both the pressure and suction surfaces, film cooling augments Nusselt number. Though augmented, Nusselt number follows the same trend as the uncooled blade. This type of distribution has been noted due to showerhead cooling by Ames[4] and Turner *et al.*[8]. At the leading edge, stagnation effects provide for the largest values in Nusselt number and begins to decrease as the boundary layer is established and grows. An increase in the

blowing ratio also leads to an increase in Nusselt number. This trend has been seen widely in literature such as references [4, 5, 7, 8, and 9]. At the blowing ratio of 1.0, film cooling increases Nusselt number by 10% to 18% over the uncooled case. Blowing ratio of 1.5 provides more Nusselt number augmentation--ranging from 10% to 29%. At the gage location just downstream of the cooling hole row on the pressure side, the blowing ratio of 1.5 provides a similar value of Nusselt number to that of the blowing ratio of 1.0. This could indicate jet liftoff or a spanwise variation in effectives at this blowing ratio on the pressure side.

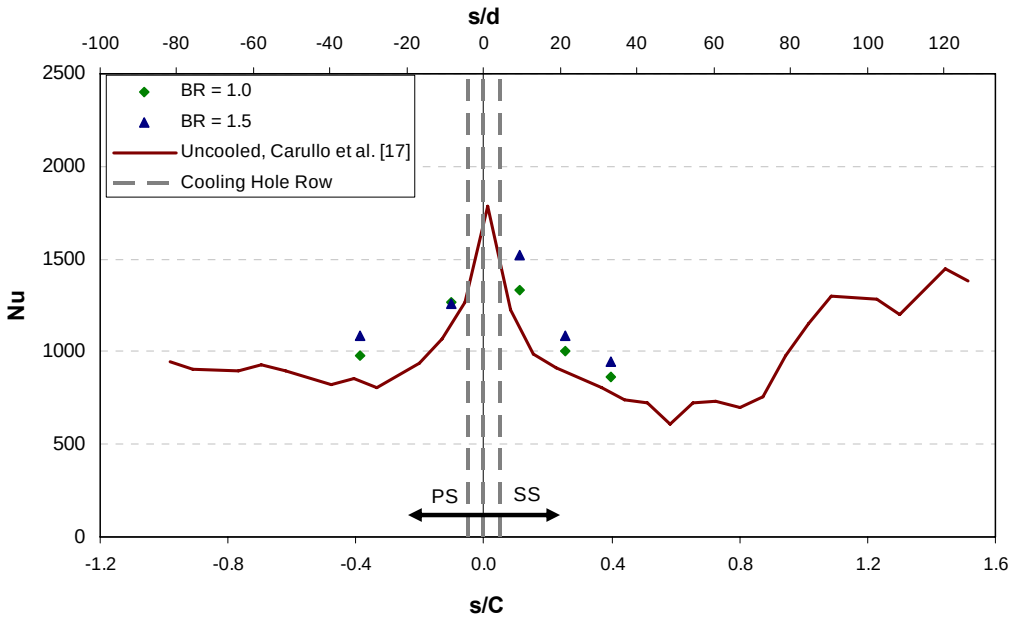

Figure 10. Effect of blowing ratio on Nusselt number at M_e=0.78.

It can be noted from Figure 11 that there is an increasing trend in Nusselt number augmentation on the pressure surface and a decreasing trend of augmentation on the suction surface. The decreasing trend in augmentation on the suction surface can be explained by the diminishing performance of the film cooling as the jet disperses downstream and the thickening of the boundary layer. While there are fewer measurement locations on the pressure surface, it can be speculated that the increase of augmentation on the pressure side could be due to the fact that the pressure side is a concave surface. On a concave surface, the jet will have more of a tendency to stay close to the wall and interact with the freestream flow, thus increasing Nusselt number

augmentation at higher blowing ratios. Bogard and Thole [2] Taylor-Görtler vortices can also form on a concave surface--increasing coolant and freestream interaction Bogard and Thole [2]. This increased interaction could cause the increasing Nusselt number augmentation.

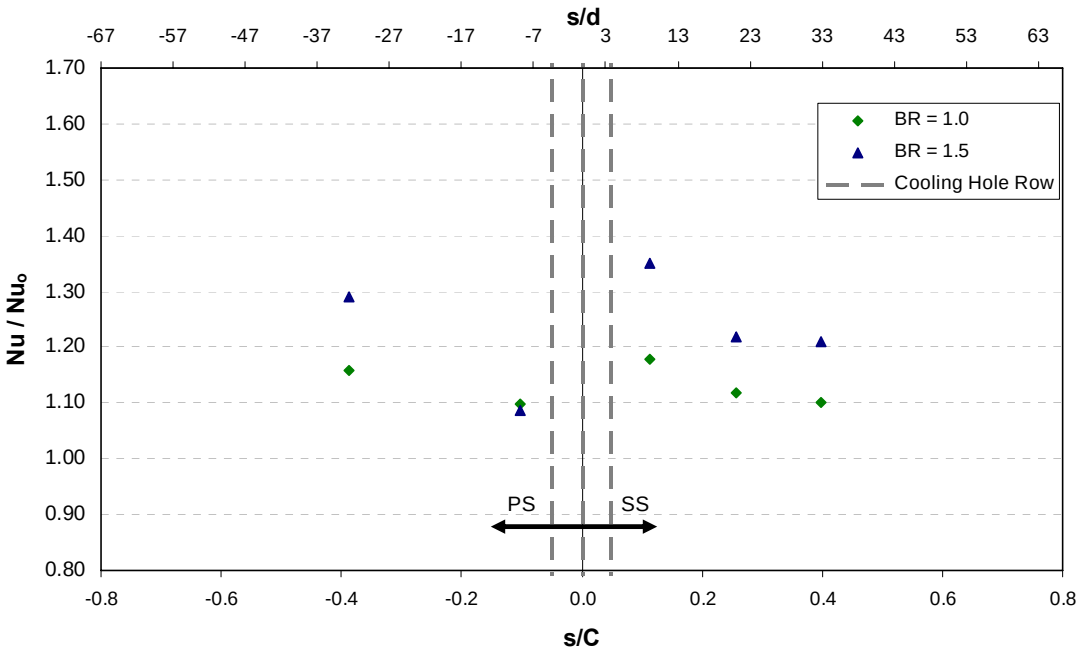

Figure 11. Effect of blowing ratio on Nusselt number augmentation at M_e=0.78.

The effectiveness distribution for M_e=0.78 is provided in Figure 12. The effectiveness decreases in an exponential fashion as the distance from coolant injection increases. Data from this study follows the same trend as effectiveness obtained from the pressure sensitive paint technique on the same blade geometry by Zhang *et al.*[16]. The values of the data are within the experimental uncertainty bracket of each other. Just downstream of injection on the pressure side, there is a decrease in effectiveness with an increase in blowing ratio. Coupled with the trend observed from Figure 10, this could indicate a jet liftoff or spanwise variation of effectiveness on the pressure side at this blowing ratio.

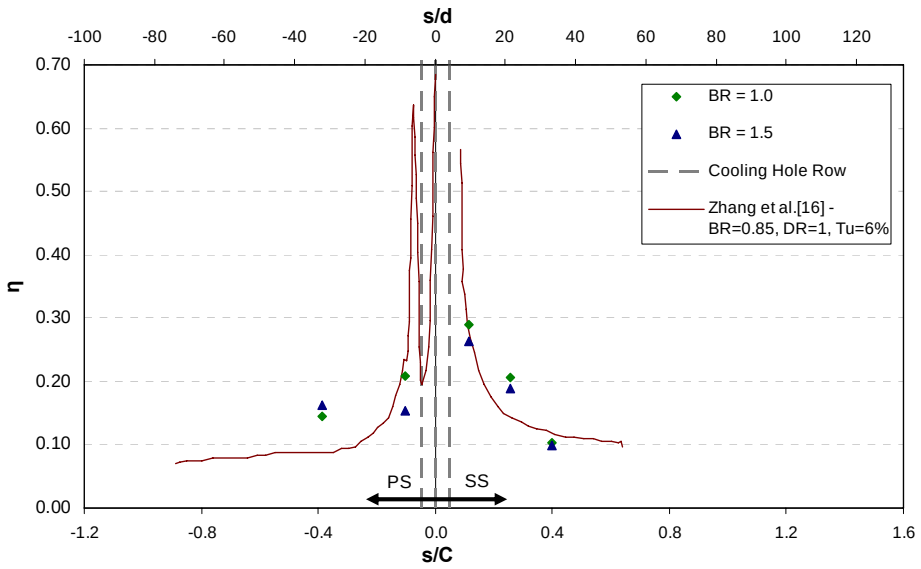

Figure 12. Effect of blowing ratio on effectiveness M_e=0.78.

Effect of Blowing Ratio at M_e=1.01

The Nusselt number distribution and augmentation plots for the exit Mach number of 1.01 are provided in Figures 13 and 14, respectively. At this Mach number, film cooling also augments Nusselt number over the no coolant case. At blowing ratio of 1.5 just downstream of injection on both the pressure and suction sides, the Nusselt numbers for the high blowing ratio are similar or below those of the lower blowing ratio. Jet liftoff on both the pressure and suction sides could be indicated by this behavior. Rigby *et al.* [13] has documented jet liftoff between a blowing ratio of 1.0 and 1.5 with Schlieren photography. On the suction side, the heat transfer coefficient is augmented by film cooling more at this Mach number than at the design Mach number of 0.78. Nusselt number augmentation ranges from 5% to 22% at the blowing ratio of 1.0. At the higher blowing ratio where there is evidence of jet liftoff, the lowest Nusselt was 7% below that of the uncooled case. At the other measurement locations, at a blowing ratio of 1.5, the augmentation ranged from 13% to 27%.

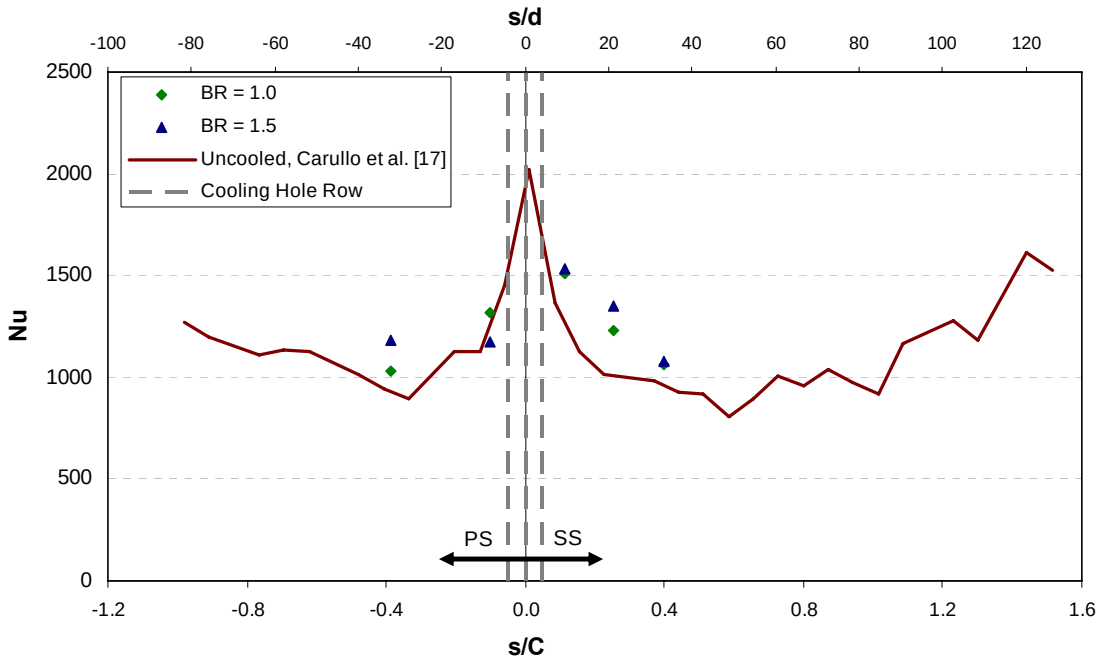

Figure 13. Effect of blowing ratio on Nusselt number at M_e=1.01.

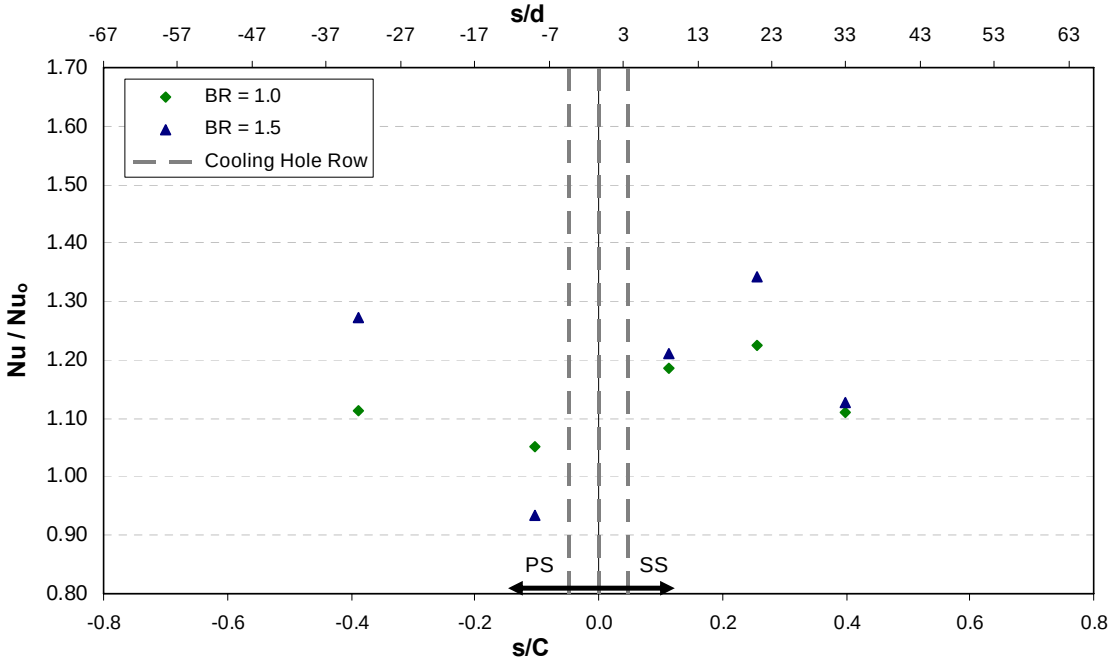

Figure 14. Effect of blowing ratio on Nusselt number augmentation at M_e=1.01.

The film cooling effectiveness distribution is provided in Figure 15. At the blowing ratio of 1.5 just downstream of injection on both the pressure and suction side, there is a large decrease in effectiveness with the increase of blowing ratio from 1.0 to

1.5. Coupled with the lack of heat transfer augmentation for this blowing ratio at this Mach number, this could indicate a jet liftoff.

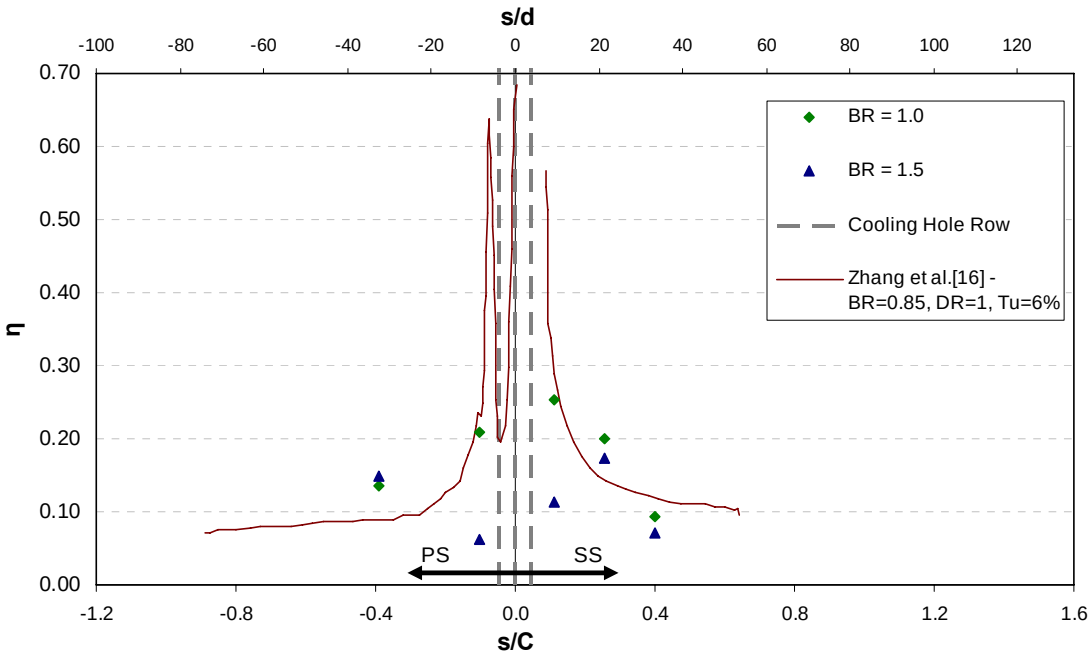

Figure 15. Effect of blowing ratio on effectiveness M_e=1.01.

Effect of Mach Number

In the current work, Mach and Reynolds number were coupled, so increasing the Mach number from 0.78 to 1.01 increased the Reynolds number from 800,000 to 1,100,000. Figures 16 and 17 show the effect of increasing the Mach number with blowing ratio of 1.0 and 1.5, respectively. Data in these figures are compared with data from the uncooled experiments by Carullo *et al.* [17]. Just as increasing the Reynolds number in the uncooled situation leads to augmentation of Nusselt number in the uncooled case, it augments the Nusselt number in the film cooled case. This effect was documented by Turner *et al.*[8]. While the increasing Reynolds number increases the Nusselt number everywhere on the blade at M_e=1.01, just downstream of the cooling hole injection on both the pressure and suction surface the highest Mach number yields a similar value of Nusselt number. This is, again, possibly due to jet liftoff at this condition.

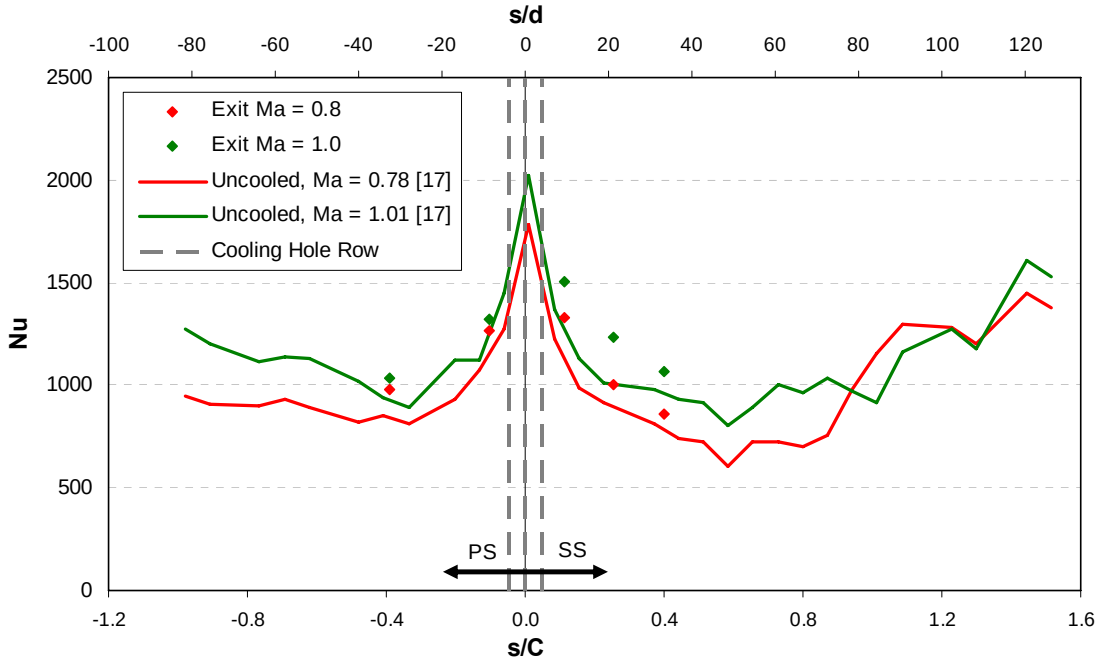

Figure 16. Effect of Mach number on Nusselt number at *BR*=1.0.

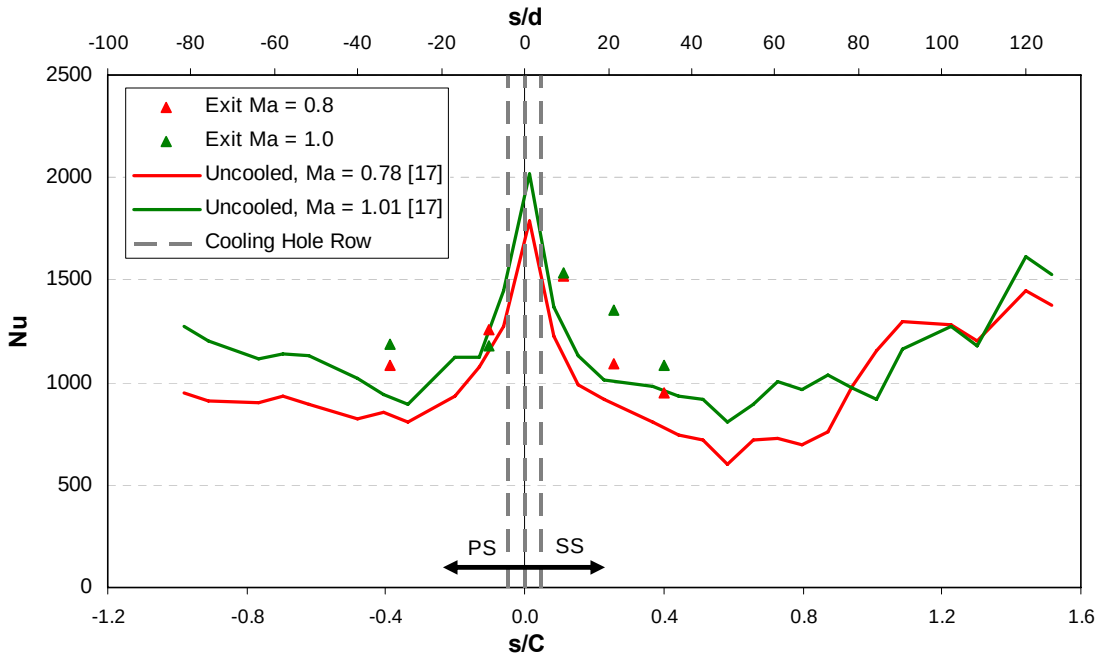

Figure 17. Effect of Mach number on Nusselt number at *BR*=1.5.

The effect of varying Mach number on film cooling effectiveness is presented in Figures 18 and 19 for blowing ratios of 1.0 and 1.5 respectively. At M_e=0.78 the effect of Mach number on effectiveness seems to be negligible. Results of Ames [4] showed a

greater effect of coolant injection rate on effectiveness than changing Reynolds number. However, at M_e=1.01 and BR=1.5, where there is evidence of jet liftoff, a large decrease in effectiveness happens just downstream of the coolant injection. Figure 19 shows that, while liftoff may be starting to occur on the pressure side at M_e=0.78, there is a much more definite effect when the Mach number is increased to 1.01.

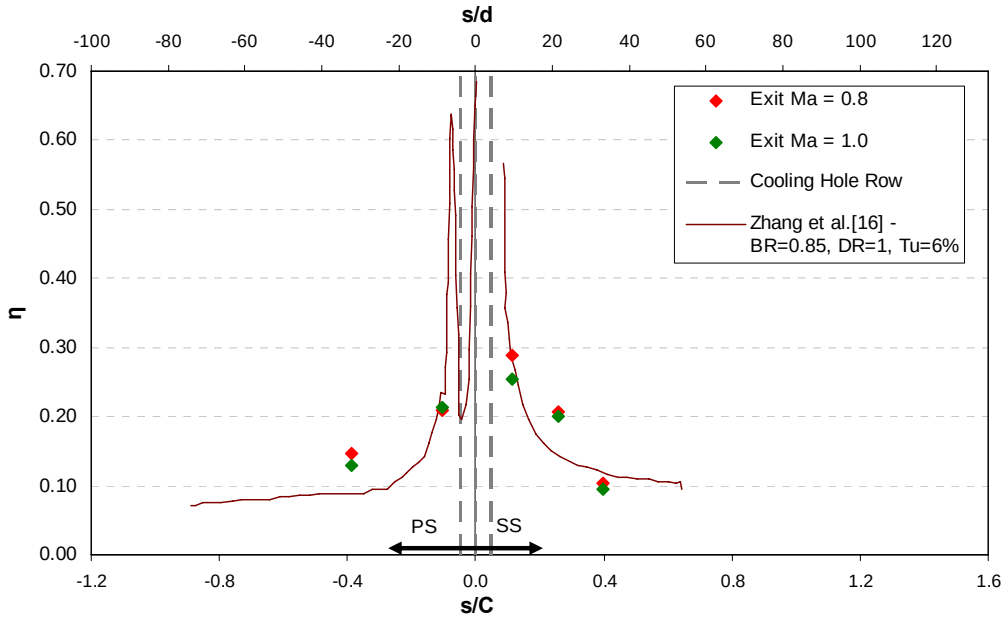

Figure 18. Effect of Mach number on effectiveness number at BR=1.0.

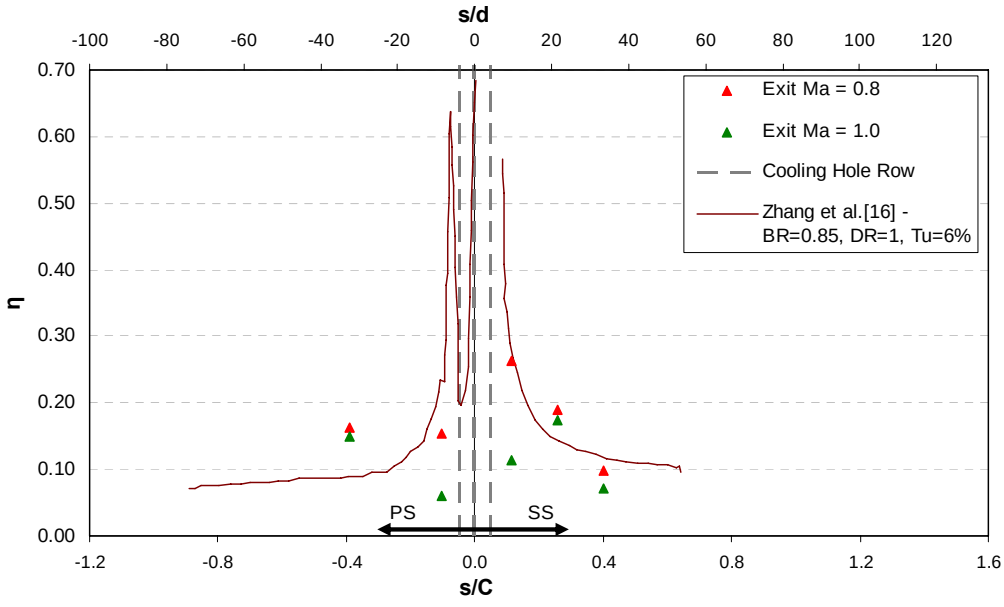

Figure 19. Effect of Mach number on effectiveness number at BR=1.5.

Net Heat Flux Reduction

Film cooling performance is a balance between adiabatic wall temperature reduction and heat transfer coefficient augmentation. While film cooling reduces the driving temperature of heat transfer, it can unfortunately increase heat transfer's scaling factor. In order to determine the successfulness of a film cooling scheme, it is important to examine the net heat flux reduction of the injected coolant. This can be described by

$$\Delta q''_{red} = 1 - \frac{q''}{q''_o} = 1 - \frac{h}{h_o}\left(1 - \frac{\eta}{\phi}\right) \tag{9}$$

where the overall film coolant performance is

$$\phi = \frac{T_w - T_r}{T_c - T_r} \tag{10}$$

Overall film cooling performance can vary over the surface of the blade, but typically is within the range of 0.5-0.7. A value of ϕ=0.6 has been chosen for this analysis. This value has been used by Mehendale *et al.*[6] in a low speed facility and Drost *et al.* [9]in a high speed facility.

The net heat flux reduction distribution provided by this scheme of showerhead film cooling is provided in Figures 20 and 21 for M_e=0.78 and 1.01, respectively. For M_e=0.78, a net heat flux reduction is achieved over the entire measurement domain for both blowing ratios. However, *BR*=1.0 provides for a greater heat flux reduction at all points because increased boundary disturbance at *BR*=1.5 results in greater Nusselt number augmentation. Drost and Bölcs [9] also showed that higher blowing ratios can increase heat load. At the high Mach number, *BR*=1.0 also provides for a net heat flux reduction everywhere on the blade. However, *BR*=1.5 provides low net heat flux reduction on the suction side and less reduction than the *BR*=1.0 on the pressure side. The *BR*=1.0 provides for better net heat flux reduction over the entire measurement domain at both freestream conditions tested than the *BR*=1.5.

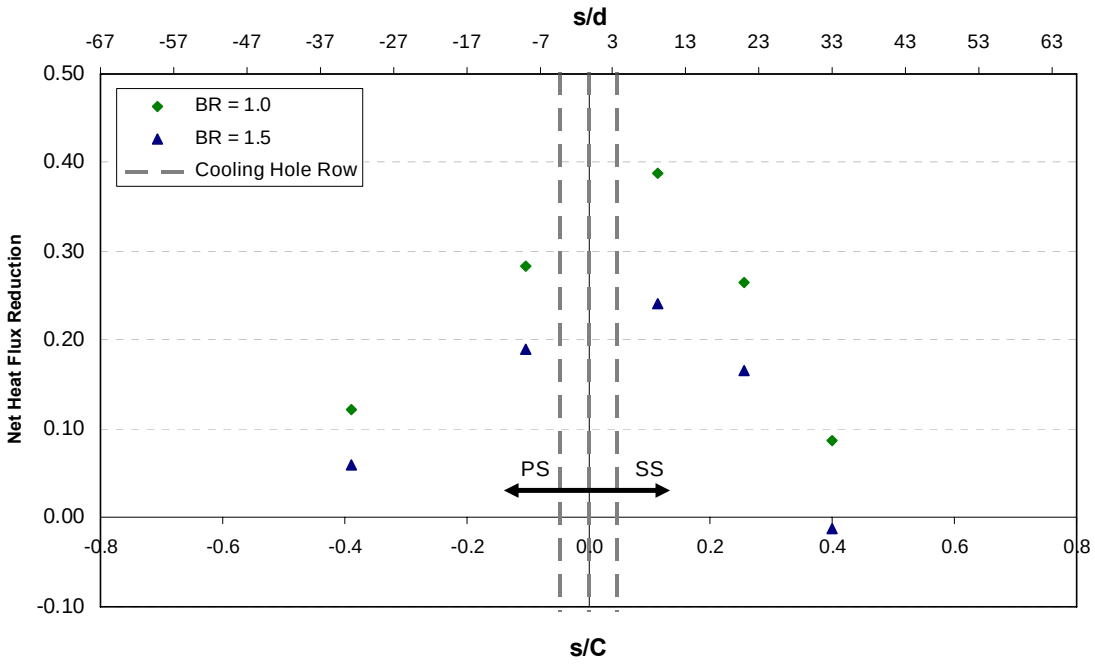

Figure 20. Net heat flux reduction for M_e=0.78.

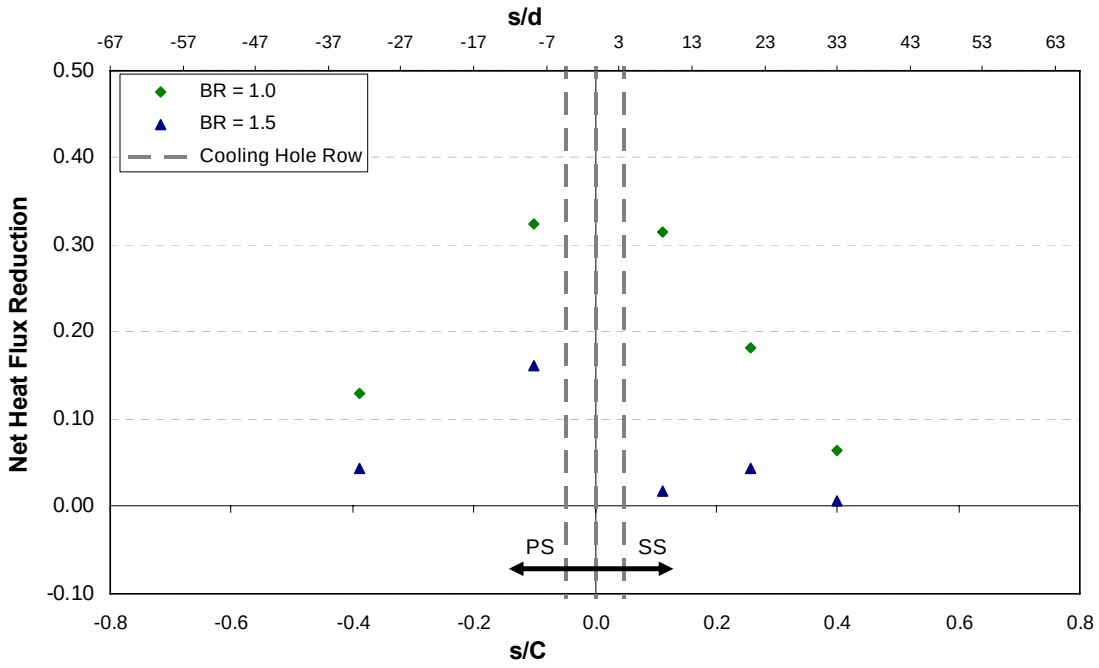

Figure 21. Net heat flux reduction for M_e=1.01.

Conclusion

A film cooled blade was tested at engine representative conditions in a transient temperature, heated, blowdown wind tunnel. Two exit Mach numbers were tested, M_e=0.78 and 1.01 at an inlet freestream turbulence intensity of 12%, with an integral LS/P=0.26. A showerhead cooling scheme of three rows of cooling holes was tested at blowing ratios of *BR*=0.6, 1.0, and 1.5 and a density ratio of *DR*=1.7. Nusselt number and film cooling effectiveness distributions were presented in the showerhead region over a range of s/d=-32 on the pressure side to s/d=33 on the suction side of the blade

At the lowest blowing ratio tested, *BR*=0.6, ingestion of freestream flow was seen to occur and for this reason, results were not presented at this test condition. At blowing ratios of 1.0 and 1.5, film cooling resulted in a Nusselt number augmentation with the highest blowing ratio providing the highest augmentation. Comparing the same blowing ratio setting at different Mach numbers showed that an increase in Reynolds number augmented heat transfer coefficient in a film cooled environment. At the highest Mach number tested, the blowing ratio of 1.5 showed evidence of jet liftoff.

Both the blowing ratios of 1.0 and 1.5 provided a net heat flux reduction over the measurement domain at each Mach number tested. The blowing ratio of 1.0 provided for superior net heat flux reduction at both freestream Mach numbers.

The data from this work was compared to effectiveness levels attained on this geometry using the pressure sensitive paint technique by Zhang *et al.*[16]. The results showed similar levels and trends over the measurement domain. Results were also compared to the uncooled heat transfer distribution provided by Carullo *et al.* [17]. The trends observed in the results of this work have compared favorably with those seen in the literature on this subject.

Acknowledgements

The authors would like to thank Solar Turbines for the funding and support provided to this project, and to Jeff Carullo for all of his help. Thanks also to Drs. Mark Polanka and Richard Anthony of the Air Force Research Laboratory for the manufacture of the Platinum thin film gages.

References

[1] Goldstein, R. J., "Film Cooling," Measurements in Heat Transfer, Washington, D.C.: Hemisphere Pub. Corp., 1976, pp 321-379

[2] Bogard, D.G., and Thole, K.A., "Gas Turbine Film Cooling," *Journal of Propulsion and Power,* Vol. 22, No. 2, 2006, pp. 249-270

[3] Han, J., Dutta, S., and Ekkad, S, Gas Turbine Heat Transfer and Cooling Technology, New York: Taylor & Francis, 2000

[4] Ames, F.E., 1996, "Experimental Study of Vane Heat Transfer and Film Cooling at Elevated Levels of Turbulence," NASA CR-4633, 1996

[5] Ou, S., Han, J.-C., Mehendale, A.B., Lee, C. P., "Unsteady Wake Over a Linear Turbine Blade Cascade With Air and CO_2 Film Injection: Part I—Effect on Heat Transfer Coefficients," *Journal of TurboMachinery*, Vol. 116, 1994, pp. 721-729

[6] Mehendale, A.B., Han, J.-C., Ou, S., Lee, C. P., "Unsteady Wake Over a Linear Turbine Blade Cascade With Air and CO_2 Film Injection: Part II—Effect on Film Effectiveness and Heat Transfer Distributions," *Journal of TurboMachinery*, Vol. 116, 1994, pp. 730-737

[7] Ekkad, S.V., Mehendale, A.B., Han, J.-C., Lee, C.P., "Combined Effect of Grid Turbulence and Unsteady Wake on Film Effectiveness and Heat Transfer Coefficient of a Gas Turbine Blade With Air and CO_2 Film Injection," *Journal of TurboMachinery*, Vol. 119, 1997, pp. 594-600

[8] Turner, E.R., Wilson, M.D., Hylton, L.D., Kaufman, R.M., "Turbine Vane External Heat Transfer: Vol. 1: Analytical and Experimental Evaluation of Surface Heat Transfer Distributions with Leading Edge Showerhead Film Cooling," NASA CR-174827, 1985

[9] Drost, U., and Bölcs, A., "Investigation of Detailed Film Cooling Effectiveness and Heat Transfer Distribution on a Gas Turbine Airfoil," *Journal of TurboMachinery*, Vol. 121, 1999, pp. 233-242

[10] Guo, S.M., Lai, C.C., Jones, T.V., Oldfield, M.L.G., Lock, G.D., Rawlinson, A.J., "The Application of Thin film Technology to Measure Turbine-Vane Heat Transfer and Effectiveness in a Film-Cooled, Engine-Simulated Environment," *International Journal of Heat and Fluid Flow*, Vol. 19, 1998, pp. 594-600

[11] Piccini, E., Guo, S.M., and Jones, T.V., 2000, "The Development of New Heat Transfer Gauge for Heat Transfer Facilities," *Measurement Science Technology*, Vol. 121, pp. 342-349.

[12] Camci, C., Arts, T., "An Experimental Convective Heat Transfer Investigation Around a Film-Cooled Gas Turbine Blade," *Journal of TurboMachinery*, Vol. 112, 1990, pp. 497-503

[13] Rigby, M.J., Johnson, A.B., Oldfield, M.L.G., "Gas Turbine Rotor Blade Film Cooling With and Without Simulated NGV Shock Waves and Wakes," ASME 90-GT-78

[14] Abhari, R.S., and Epstein, A.H., "An Experimental Study of Film Cooling in a Rotating Transonic Turbine," *Journal of TurboMachinery*, Vol. 116, 1994, pp. 63-70

[15] Smith, D.E., Bubb, J.V., Popp, O., Grabowski, H. III, Diller, T.E., Schetz, J.A., Ng, W.F., "An Investigation of Heat Transfer in a Film Cooled Transonic Turbine Cascade, Part I: Steady Heat Transfer," ASME 2000-GT-202

[16] Zhang, L., and Moon, H.K., "Turbine Blade Film Cooling Study-The Effects of Showerhead Geometry," Proc. GT2006 ASME Turbo Expo 2006, ASME GT2006-90367

[17] Carullo, J.S., Nasir, S., Cress, R.D., Ng, W.F., Thole, K.A., Zhang, L.J., and Moon, H.K., 2007, "The Effects of Freestream Turbulence, Turbulence Length Scale, and Exit Reynolds Number on Turbine Blade Heat Transfer in a Transonic Cascade," ASME GT-2007-27859.

[18] Carullo, J.S., 2006, "Effects of Freestream Turbulence, Turbulence Length Scale, and Reynolds Number on Turbine Blade Heat Transfer in a Transonic Cascade," Master's Thesis, Virginia Tech.

[19] Colban, W., Gratton, A., Thole, K.A., "Heat Transfer and Film-Cooling Measurements on a Stator Vane With Fan-Shaped Cooling Holes," *Journal of TurboMachinery*, Vol. 128, 2006, pp. 53-61

[20] Cress, R.D., 2006, "Turbine Blade Heat Transfer Measurements in a Transonic Flow Using Thin film Gages," Master's Thesis, Virginia Tech.

[21] Moffat, R. J., 1988, "Describing Uncertainties in Experimental Results," *Exp. Thermal and Fluid Science*, 1988, pp. 3-17.

[22] Brown, K.H., Coleman, H.W., and Steele, W.G., "Estimating Uncertainty Intervals for Linear Regression," Proceedings of the American Institute of Aeronautics and Astronautics 33rd Aerospace Sciences Meeting and Exhibit, Reno, NV January 1995 AIAA 95-0796

[23] Smith, A.C., Nix, A.C., Diller, T.E., Ng, W.F., "The Unsteady Effect of Passing Shocks on Pressure Surface Versus Suction Surface Heat Transfer in Film-Cooled Transonic Turbine Blades," Proc. GT2003 ASME Turbo Expo 2006, ASME GT2003-38530

Appendix A: Film Cooling System

This appendix describes the construction and operation of the film cooling system in greater depth.

Cooling System Setup and Operation

The system is an adaptation of the one used by Smith *et al*. [15]. A schematic of the system is provided in Figure A-1 and a photograph is provided in Figure A-2. The 5 HP Ingersoll Rand compressor is located outside of the tunnel laboratory in a storage shed and connected to the storage tank by copper tubing. Air from the compressor is filtered and dried to below 4 percent relative humidity. The storage tank is charged to a pressure of 120 psi. Because the volume of the tank is large compared to the amount of coolant used, there is minimal "blowdown" during a tunnel run. The flowrate of air to the blade is controlled by a pneumatic control valve, manufactured by BadgerMeter inc. After passing through the control valve, massflow is measured using an orifice plate. The air passes through a coil of copper tubing immersed in liquid nitrogen. After the air is cooled, it reaches the blade plenum and is ejected over the blade to provide film cooling. A fitting was designed to provide air through the test section window into the plenum. The fitting, shown in Figure A-3, connects to copper tubing on one end and uses an o-ring to provide for a face seal against the blade. This provides air to the plenum without leakage.

The control valve is a proportional type control with the valve opening proportionally to the amount of air pressure that is applied to it. Shop air provides the pressure needed to open the valve. A signal pressure is supplied by an electro-pneumatic converter that converts a voltage input to a proportional pressure output. Increasing the signal pressure will increase the amount of air that is allowed to pass through the valve.

Air is supplied to the plenum at a constant pressure throughout the run. Before the tunnel is operated, the supply of air to the plenum is set with the control valve. A readout of the plenum pressure, measured with a pitot-static probe, is monitored while adjusting the control valve. When the desired pressure is reached, the tunnel control is started. This provides a constant blowing ratio as shown in Figure 8.

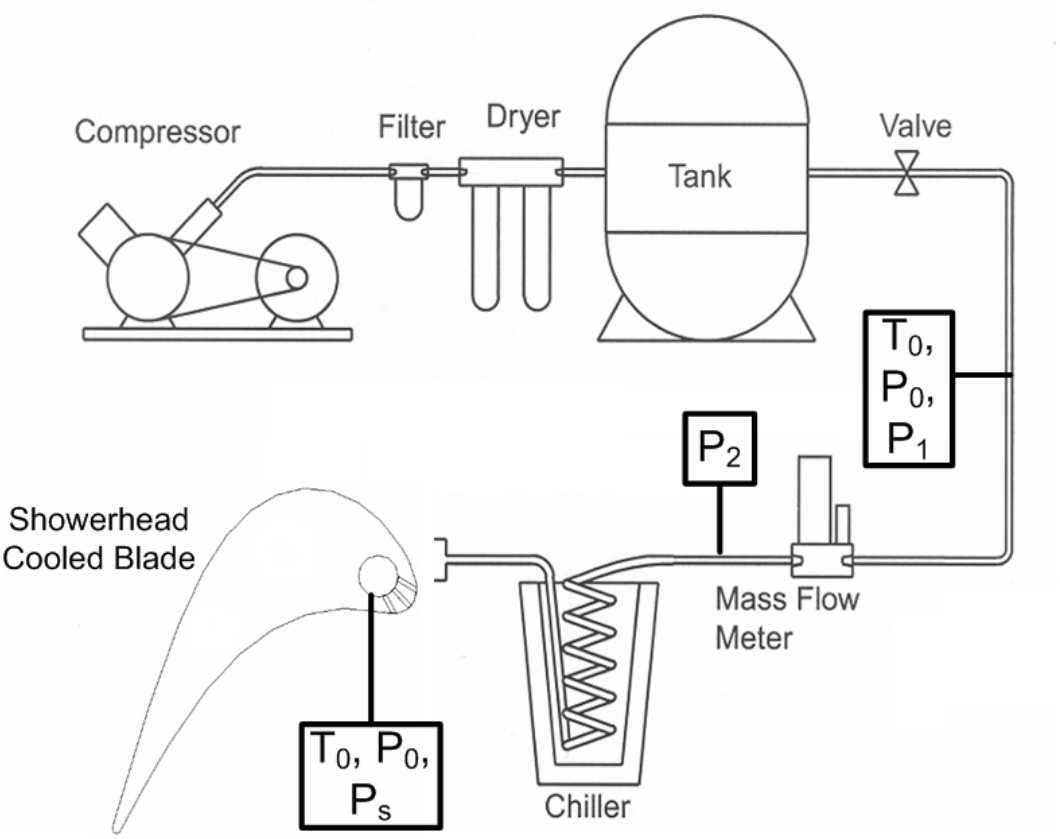

Figure A-1. Film cooling system schematic. Locations of pressure and temperature measurements are indicated.

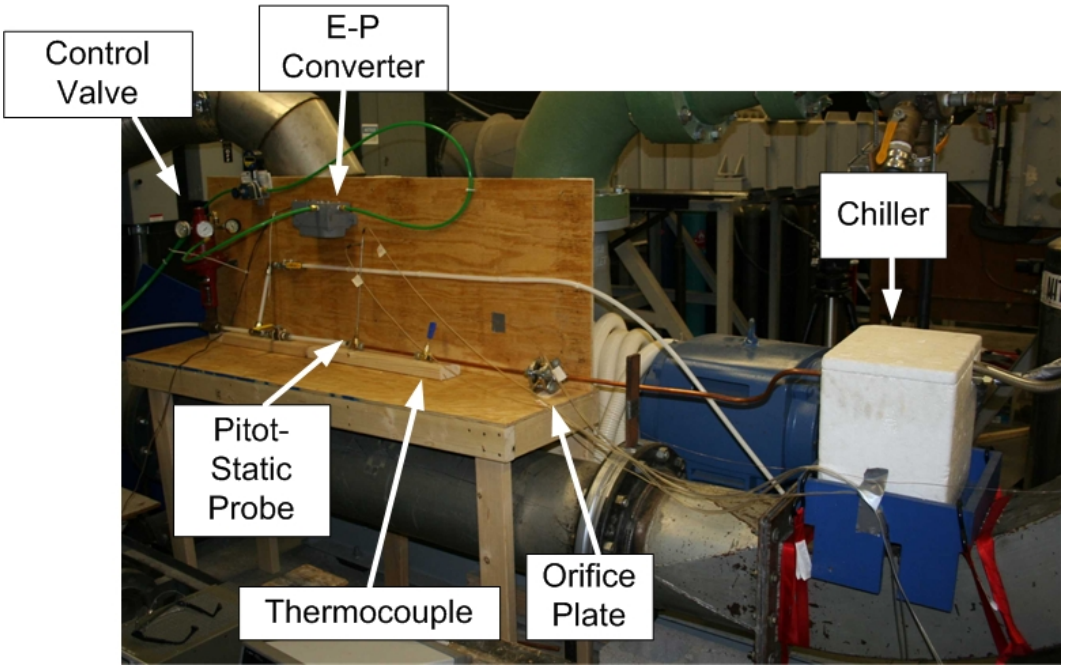

Figure A-2. Photograph of film cooling supply.

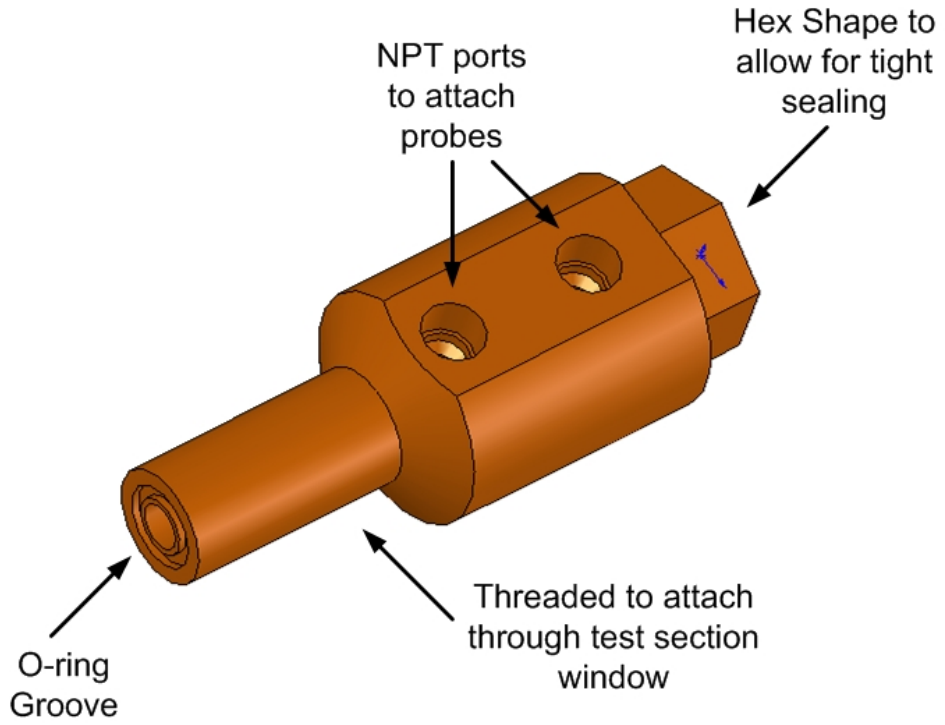

Figure A-3. Coolant supply fitting.

Measurements and Calculations

This section describes the instrumentation used and the equations needed to calculate the film cooling parameters. Equation 2 describes the calculation of blowing ratio. The massflow into the plenum was measured by the orifice plate and calculated by

$$\dot{m}_c = C_d A_{op} \sqrt{2\rho\Delta P} \tag{A-1}$$

where C_d is the discharge coefficient of 0.62, A_{op} is the area of the orifice plate of 3.95 x 10^{-5} m^2, ρ is the density of air, and ΔP is the pressure drop across the plate. A pitot-static probe and thermocouple upstream of the orifice plate provide the measurements needed to calculate the density of the air through the orifice plate. Their locations are shown in Figures A-1 and A-2.

A pitot-static probe was placed at the entrance to the film cooling plenum to provide for the pressure measurement necessary to set the coolant flow conditions prior to a test run. Pressure measurements from this probe are also used to calculate the density ratio. The temperature of the coolant was measured by a thermocouple inserted into the plenum near the midspan of the blade. Because of the low thermal conductivity of the

Macor blade, it was assumed that the temperature of the plenum was the same as the temperature of the coolant as it exited the coolant holes.

Checklists were used for each run to record the parameters used and provide for consistent operation. These were authored by Bolchoz and are contained in this appendix. A pre-run checklist was used to prepare for each day of tests and a tunnel run checklist was used to set and record the conditions of each run.

Date: ____/____/____ Name: _____

Pre-Run Checklist

- PSI
  - Turn on **PSI 8400** and heat up for 1 hour.
  - After 1 hour, set air bottle pressure to **100<P(psi)<120.**
  - **Disconnect trigger for calibration.**
  - **Calibrate PSI 8400**.
  - After calibration**, switch air** to tunnel control valve (P=25psi).
  - Reconnect trigger
- Film Cooling System
  - Close off open valves on **film-cooling tank** and start **compressor**.
  - Go outside and make sure that compressor is on, dryer is on, and ball valve exiting compressor is open.
  - Charge tank to 120 psi and turn off compressor.
  - Turn on **shop air** to control valve.
  - Inspect cooling instrumentation and ensure that **thermocouples/pitot probes** are in correct positions and that **everything is connected** with desired flow path set.
- Heater
  - Open **heater loop**, and turn on **fan/heater**.
  - Heat to 600°F on bottom display, and then allow heater to cool to 300°F.
  - Turn heater on again and repeat process until target of 232°F is reached on top display.
- Instrumentation
  - Turn on **DAQ and MKS transducers** and zero MKS.
  - Measure **pre-run resistances** of TFG's and record in input file.
  - Supply **10VDC(± 3mV) to Wheatstone bridge** circuit.
    - Measure with multimeter and record voltage in input file.
  - Measure Wheatstone bridge output for each gage and use potentiometers to **zero the gage** (± 0.005 mV).
- Tunnel
  - Start **tunnel compressor** and turn on **panel/tunnel computer**.
  - Get **atmospheric pressure** and enter into **input file** on computer and tunnel control software.
  - Set **tunnel objective pressure** in control software.
  - Ensure that all **clamps on tunnel windows** are secure
  - Place **safety shields** in front of tunnel windows.
- Record the overall purpose of the day's experiments in the tunnel run log.

Tunnel Run with Cooling Checklist

Test Objective: _____

Before Run:

- ☐ Open heater loop.
- ☐ Cool blade to room temperature.

Cooling System

- ☐ Ensure that cooling tank is charged to 100 psi and that compressor is off.
- ☐ Ensure that cooling is routed through chiller.
- ☐ Set voltage supply to 0V.
- ☐ Open manual and solenoid valves.

Heater

- ☐ Ensure that heater loop is open with 2 valves.
- ☐ Heat copper tubes to 232°C.
- ☐ Turn heaters off, but keep fan on.

Tunnel

- ☐ Make sure that tunnel is set to run from outside
- ☐ Set air bottle pressure to 25 psi for tunnel control valve.
- ☐ Charge tunnel tank to 140 psi.

DAQ

- ☐ Make sure that PSI is calibrated and acquiring.
- ☐ Have appropriate DAQ .vi ready to record.

Running:

- ☐ Pour _____ inches of nitrogen into the cooler.
- ☐ Start stopwatch and *slowly* increase voltage, monitoring plenum total pressure reading on MKS for initial pressure spike; then set the pressure to appropriate value _____Volts.
- ☐ At _____ seconds, cooling operator should open green heater loop valve while another operator shuts off fan.
- ☐ At _____ seconds, the other operator should open the downstream heater valve.

At this point both operators leave room, and the tunnel/DAQ should be started.

After run, record test information in log.

Notes:

Appendix B: Double-sided Gage Installation

Gage Mounting. Double-sided gages were constructed from platinum thin film gages manufactured by the Air Force Research Laboratories and 0.5 mil thin foil thermocouples manufactured by RDF corporation. The platinum thin film gages are laid with their adhesive side up as shown in Figure B-1. The paper backing is removed from the adhesive a few gages at a time. A thin foil thermocouple is then mounted to adhesive backing of the platinum thin film gages. The sensing junction of the thermocouple is aligned to the midspan of the platinum portion of the thin film gage with the aid of a pair of tweezers. The thermocouple leads are then extended across the adhesive portion of the gage sheet. The sheet is placed over a lined substrate to provide guidance so that the thermocouple leads can be arranged parallel with each other. Figure B-1 shows a gap where two platinum gages were left without a backwall thermocouple. This area of the gage sheet corresponds to the cooling hole row locations on the leading edge of the blade.

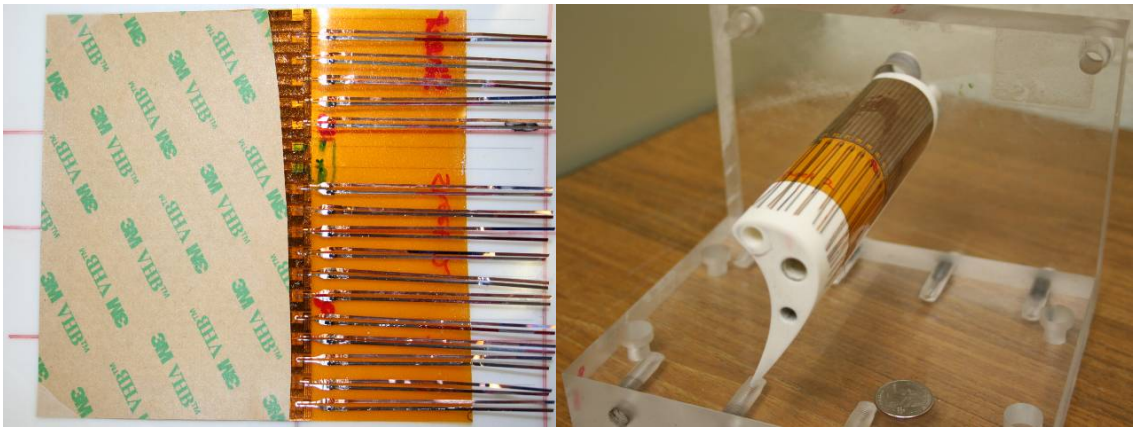

Figure B-1. Installation of thermocouples to Pt thin film gages(L). The attachment of the gage sheet to the blade(R).

Once the entire sheet of platinum thin film gages had been instrumented with backwall thermocouples, the sheet was applied to the showerhead film cooled blade. The midspan location of the blade was marked and the gages were aligned starting with the "empty" gages at the leading edge of the blade. The sheet was slowly wrapped around the blade on the suction side. Care was taken to apply the sheet slowly and to apply pressure in a rubbing fashion towards the blade endwalls away from the midspan to prevent air from being trapped beneath the gage sheet. After the suction side gages had

been successfully installed, the blade was rotated in its stand and the process was repeated on the pressure side of the blade.

Film Cooling Holes. Once the gage sheet had been installed, the cooling holes had to be placed in the gage sheet. Holes had previously drilled through the surface of the blade into the cooling plenum, but were covered up when applying the gage sheet. On one half of the span of the blade, the copper leads of the thin film gages covered up the cooling holes. This copper lead was carefully scraped away using an X-ACTO® blade. This process was able to be completed without roughening the kapton surface.

A soldering iron was equipped with a thin, conical tip and heated to a setting of ~700ºF. The soldering iron was aligned to the spanwise angle of the cooling hole. Then, the heated soldering tip was used to pierce a hole in the kapton. A heated soldering iron was used because it produced a hole while preventing the kapton from ripping. A drill bit the same diameter as the cooling hole was placed in a pen vise and then used to clear the kapton material from the cooling hole. If a "hanging-chad" of kapton material was left in the cooling hole, the back end of the drill bit(the part normally inserted into the drill chuck) was used to cut and push the kapton through the hole into the plenum. The kapton material was cleared from the plenum and each cooling hole was visually inspected to insure that there was no blockage.

Lead Wires. Lead wires were soldered to the platinum thin film gage following the procedure outlined in Carullo[18]. The leads were covered with JB weld to physically secure them and protect them from the tunnel flow. The blade was then placed inside an oven for calibration of the thin film gages. The calibration procedure is discussed by Cress [20]. After calibration, the blade was mounted to the clear, Lexan test section window. A layer of silicon caulk was applied over the JB weld to secure the blade to the window and to provide for a smooth surface for the flow to go over.

An aluminum "insert" was attached to the thermocouple side of the blade. This insert allowed for the blade to be removed from the test section without disturbing the gage configuration. An image of this setup is provided in B-2. The thermocouple leads extended off the span of the blade in the opposite spanwise direction as the thin film gages. Thermocouple wires were inserted through holes in the "insert" and soldered to the leads. Soldered leads were covered with a layer of silicon caulk to protect them from

the elements and seal the tunnel test section. Figure B-3 shows the gages mounted with the lead wires soldered and shows the instrumented blade installed into the cascade.

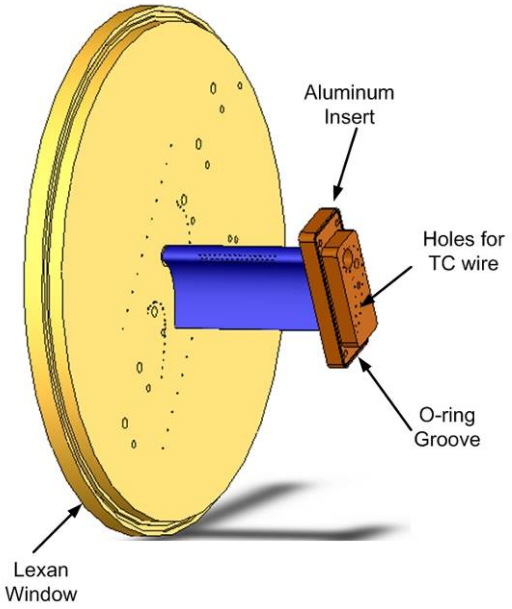

Figure B-2. Blade with lexan window and aluminum insert.

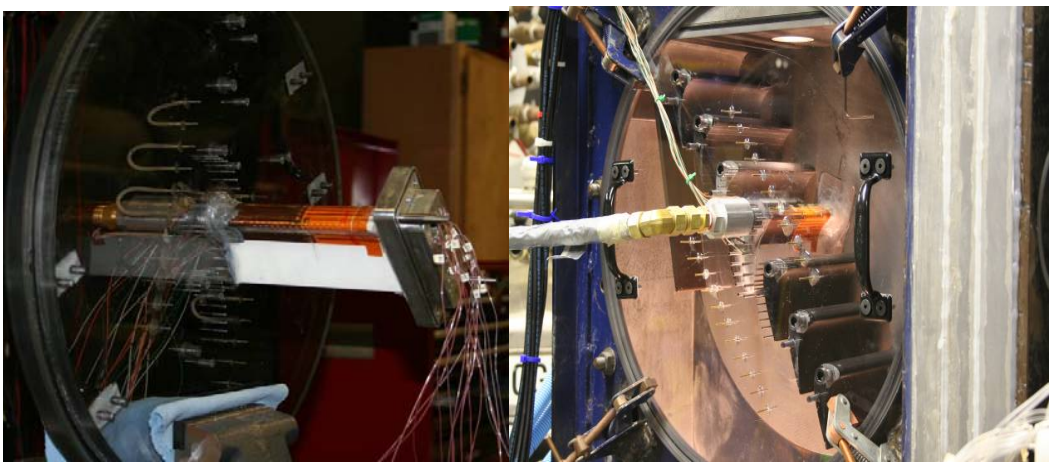

Figure B-3. Photographs of installed test hardware. Lead wires attached to thin film gages and thermocouples(L). Instrumented blade installed to test section with film cooling supply shown(R).

Appendix C: Material Properties Calibration

This appendix describes the process used to calibrate for the material properties of the double-sided gage used in this work. Figure C-1 shows an expanded schematic of this gage.

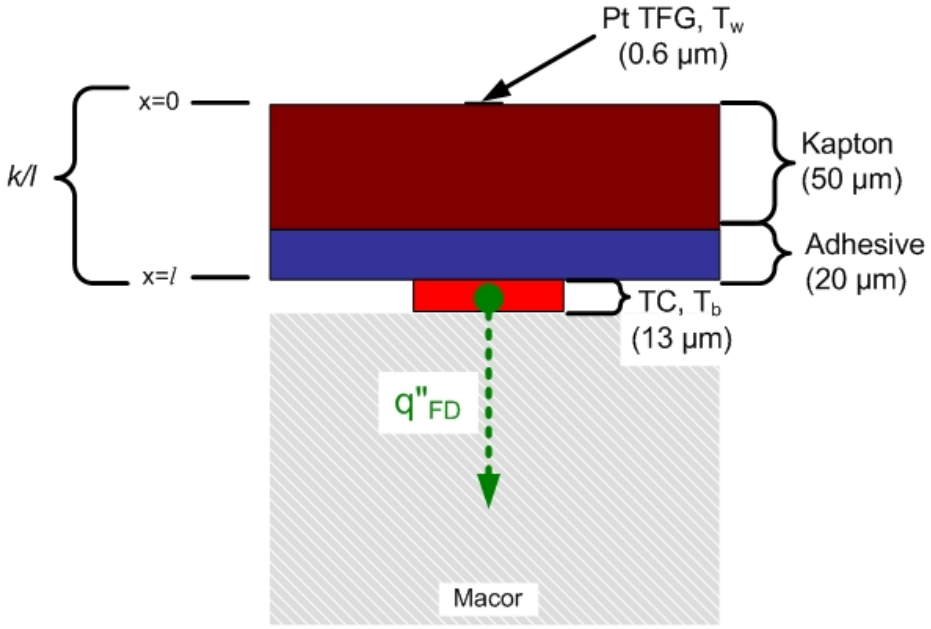

Figure C-1. Expanded schematic of the double-sided gage.

The heat flux the blade experiences during a typical tunnel run depends on location of the blade but can range from 12 kW/m^2 to 30 kW/m^2. A step input of heat flux was imposed on the gage by a laser, and the response time of the gage was determined to be about 30 ms. This response time was also seen in a double-sided gage described by Ewing *et al.*[C-1]. This heat flux gage measures temperatures on either side of a kapton and adhesive layer that is around 70 μm thick. Since this gage measures a high heat flux over a very thin layer and possesses a fast response time, it can be assumed that the temperature profile through the gage is linear. The heat flux through the gage can be described by

$$q'' = k/l\,(T_w - T_b) \qquad \text{(C-1)}$$

where T_w is the platinum thin film gage temperature, T_b, is the backwall thermocouple temperature, and k/l is the thermal conductivity divided by the gage thickness.

Cress [20] developed a one-dimensional finite difference code to find the heat flux into the blade using a platinum thin film gage as the surface temperature. This code

was adapted to solve for the heat flux into the macor blade using the backwall thermocouple, T_b, as the input. With the heat flux as a known and assuming that the heat flux into the gage is the same as the heat flux into the blade, Equation C-1 can be arranged as

$$k/l = \frac{q''_{FD}}{(T_w - T_b)} \tag{C-2}$$

where q''_{FD} is the heat flux determined from the finite difference code.

The finite difference code is valid at locations on the blade away from the film cooling plenum during a tunnel run where film cooling is not introduced. Three heated tunnel runs at *Me*=0.78, *Tu*=2%, and no film cooling were used to provide the conditions necessary for this calibration. Three gage locations where the finite difference code was valid were analyzed to determine the *k/l* of the kapton and macor.

For three gages over three tunnel runs the k/l value was determined to be 1240 ± 90 W/m^2-K using the 95% confidence interval. Bias error was found using Moffat's [21] small perturbation method and precision error was found from gage to gage and run to run repeatability. Assuming that the adhesive layer does not change its thickness due to mounting, the conductivity of the kapton used in the current research was found to be 0.09 ± 0.006 W/m-K. Once the material properties of these gages were calibrated during an uncooled tunnel run, they could be used in a film cooled environment.

References

[C-1] Ewing, Jerrod, 2006, "Development of a Direct-Measurement Thin film Heat Flux Array," Master's Thesis, Virginia Tech

Appendix D: Uncertainty Analysis

This appendix describes how the uncertainty of of h and η were determined. Heat transfer coefficient was determined from the slope of the line fit shown in Figure D-1. Each data point has an uncertainty in its x location and y location. This uncertainty was determined within the 95% confidence interval using Moffat's [21] small perturbation method. The linear regression equation is applied to the set of data points and the equation of the line is calculated.

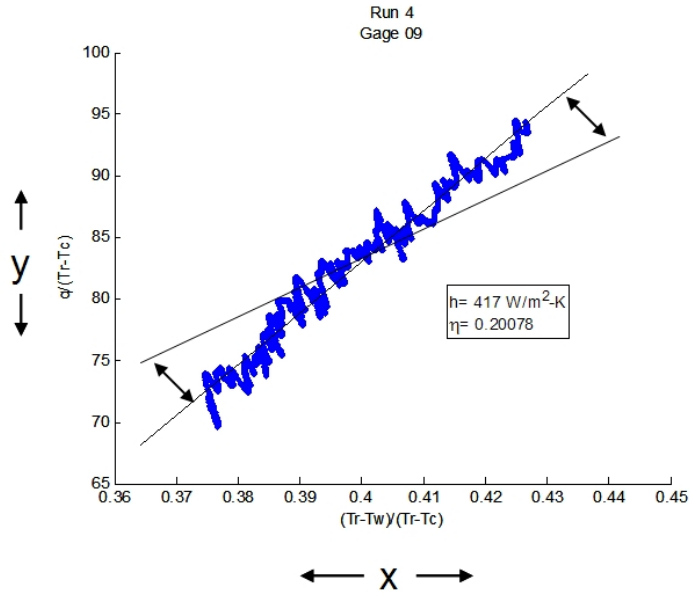

Figure D-1. Description of Uncertainty

Brown *et al.*'s [22] method was used to determine the uncertainty of the line fit through the data. The bias error in the x and y direction determined from the small perturbation method were used as an input to Brown *et al.*'s [22] analysis procedure. Covariance was assumed to be negligible. The uncertainty in the slope and x-intercept determined from this procedure is the uncertainty in h and η, respectively.

The standard linear regression equation assumes that all error is contained within the y-axis data. This happens to be a good assumption in this case because the magnitude of error in the y-axis is much greater than that in the x-axis. Reed [D-1] describes a method used to fit a line through data with error in both the x and y axis. To further validate that a fit method assuming only y-axis uncertainty was appropriate for this work, Reed's[D-1] method was used on sample data sets and slope and intercept were

compared to those found using the standard fit method. The differences in the results of the two methods was determined to be negligible. The standard regression equation was used in this work because it provided the same results as York's method without the need for iteration.

Uncertainty values for intermediate and final results are shown in Table D-1. Uncertainties in M_e, DR, and BR were determined with Moffat's [21] small perturbation method within the 95% confidence interval. Precision uncertainty for k/l was determined using run to run and gage to gage repeatability. Samples of data plotted with the uncertainty band are provided for Nusselt number and Effectiveness in Figures D-2 and D-3, respectively.

Table D-1. Uncertainty Values

Value	Uncertainty (± Percentage)
h	10
η	20
$\Delta q''_{red}$	17
k/l	7
M_e	1.3
DR	0.4
BR	1.4

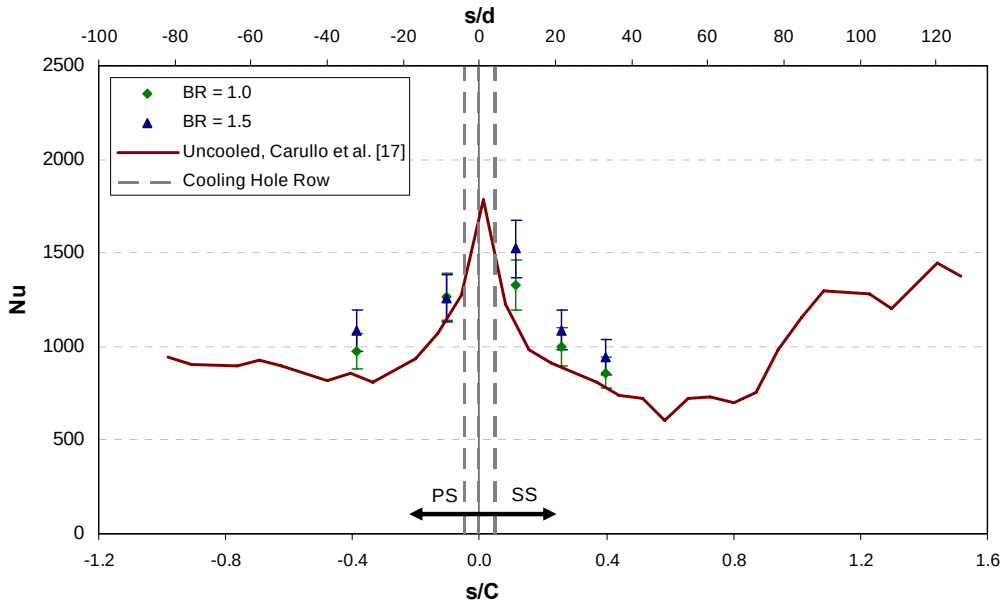

Figure D-2. Nusselt number Distribution with uncertainty included. This is Figure 9 plotted with error included.

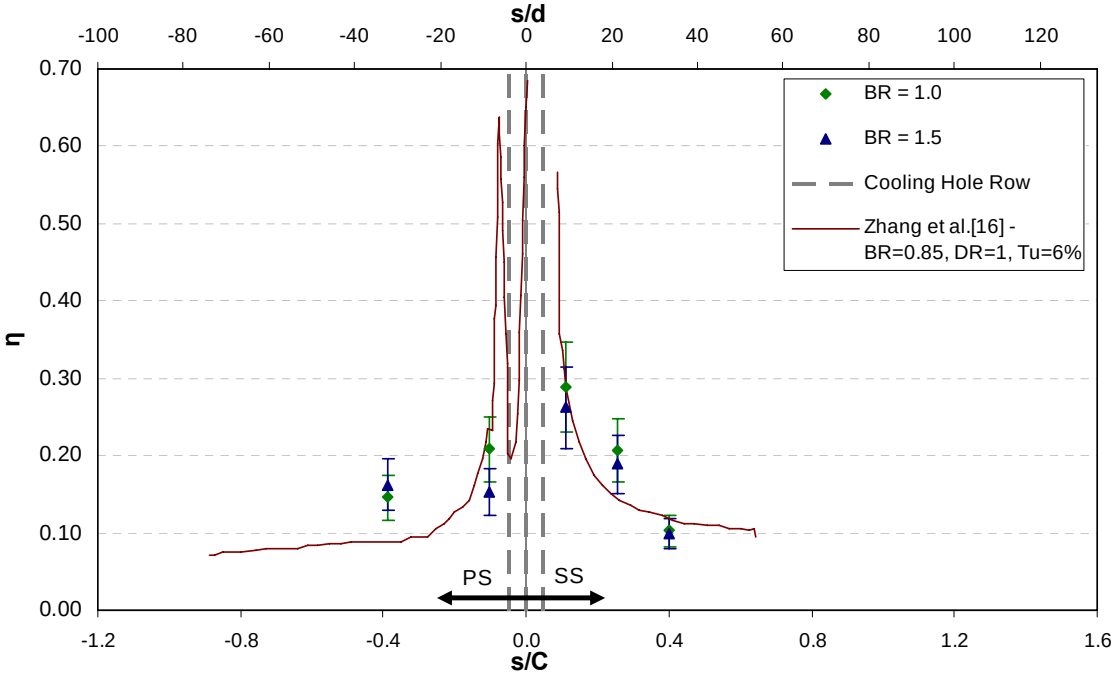

Figure D-3. Effectiveness Distribution with uncertainty included. This is Figure 11 plotted with error included.

References

[D-1] Reed, B.C., "Linear least-squares fits with errors in both coordinates," *American Journal of Physics*, Vol. 57, No. 7, 1989, pp. 642-646

Appendix E: Tabulated Results

This appendix contains results previously presented in graphical form as tabulated data for convenience.

Mach 0.78 Tabulated Results

Table E-1. M_e=0.78, Nu

s/C	*s/d*	*BR*=1.0	*BR*=1.5
0.399	33.257	860	950
0.256	21.325	1000	1090
0.113	9.392	1330	1520
-0.102	-8.507	1270	1250
-0.388	-32.372	980	1090

Table E-2. M_e =0.78, Nu/Nu_0

s/C	*s/d*	*BR*=1.0	*BR*=1.5
0.399	33.257	1.10	1.21
0.256	21.325	1.12	1.22
0.113	9.392	1.18	1.35
-0.102	-8.507	1.10	1.09
-0.388	-32.372	1.16	1.29

Table E-3. M_e =0.78, η

s/C	*s/d*	*BR*=1.0	*BR*=1.5
0.399	33.257	0.10	0.10
0.256	21.325	0.21	0.19
0.113	9.392	0.29	0.26
-0.102	-8.507	0.21	0.15
-0.388	-32.372	0.15	0.16

Table E-4. M_e =0.78, $\Delta q''_{red}$

s/C	*s/d*	*BR*=1.0	*BR*=1.5
0.399	33.257	0.12	-0.01
0.256	21.325	0.27	0.17
0.113	9.392	0.39	0.24
-0.102	-8.507	0.28	0.19
-0.388	-32.372	0.12	0.06

Mach 1.01 Tabulated Results

Table E-5. $M_e = 1.01$, Nu

s/C	*s/d*	***BR*=1.0**	***BR*=1.5**
0.399	33.257	1070	1080
0.256	21.325	1230	1350
0.113	9.392	1510	1540
-0.102	-8.507	1320	1180
-0.388	-32.372	1030	1180

Table E-6. $M_e = 1.01$, Nu/Nu_0

s/C	*s/d*	***BR*=1.0**	***BR*=1.5**
0.399	33.257	1.11	1.13
0.256	21.325	1.22	1.34
0.113	9.392	1.19	1.21
-0.102	-8.507	1.05	0.93
-0.388	-32.372	1.11	1.27

Table E-7. $M_e = 1.01$, η

s/C	*s/d*	***BR*=1.0**	***BR*=1.5**
0.399	33.257	0.10	0.07
0.256	21.325	0.20	0.17
0.113	9.392	0.25	0.11
-0.102	-8.507	0.21	0.06
-0.388	-32.372	0.13	0.15

Table E-8. $M_e = 1.01$, $\Delta q''_{red}$

s/C	*s/d*	***BR*=1.0**	***BR*=1.5**
0.399	33.257	0.06	0.01
0.256	21.325	0.18	0.04
0.113	9.392	0.32	0.02
-0.102	-8.507	0.32	0.16
-0.388	-32.372	0.13	0.04

Appendix F: Data Reduction Code

This appendix contains the MATlab mfile that was used to reduce the data. Data was saved in four files: input file, NI file, NI initial value file, and PSI file. The input file contained all of the data related to that day of testing including pre run resistances, thin film calibration constants, atmospheric pressure. It also included gage data including location, material properties, and local Mach number. All pressures were recorded by the PSI 8400 (PSI) system and were in the PSI file. Two files were recorded using the National Instruments AT-MIO-16XE-50 system(NI). A file containing the initial temperatures was recorded prior to starting any coolant. Then during testing, the NI system recorded all voltages and temperatures.

This mfile reads in all of the data files and computes all quantities of interest in this work. An option for saving the reduced data in an excel file is given. Included in this mfile are the codes needed to make plots of interest.

Code:

```
clear all
close all
clc
%format long
global N fs
%Read in data from 4 files, a daily input file, PSI 8400 output, and
%NI daq system
%temperature and voltage history in NI data and NI initial value file,
%pressures in PSI data
%%%%%%%%%%file names
p1='z:\Solar_Research\Film_Cooled\Tunnel Test\Final Blade\12_Turbulence\Mach 0_80\BR_1\';
date='04-19-07';
r1='Run';
r2='_';
r3='4';%%%%%%%%Run #
Run=[r1 r2 r3];
Rund=[r1 ' ' r3];%title for plots
NI='\NI_';
PSI='\PSI_';
p2='.lvm';
NI_file=[p1 date NI Run p2];
PSI_file=[p1 date PSI Run];
reduce='_reduced_final';
init='_init';
p3='.xls';
slash='\';
IN='Input ';
savename=[p1 date slash Run reduce p3];%name for saved excel results file
input_name=[p1 date slash IN date p3];
init_file=[p1 date NI Run init p2];
fs=1000;% NI sampling rate(Hz)
psi_fs=20;%psi sampling rate(Hz)
%%%%%%%%%%input files%%%%%%%%%%%%%
NI_data_prefilt=dlmread(NI_file);
init_data=dlmread(init_file);
PSI_data=dlmread(PSI_file,'\t',1,0);
input=xlsread(input_name,'input','B2:I17');
```

```
%%%%%%%%%%%%%%%%%%%%%%%%%%%%%%%%%%%%%%%%%%%%%%%%%%%% name for plots/saving
gagename=['Gage 01';'Gage 02';'Gage 03';'Gage 04';...
    'Gage 05';'Gage 06';'Gage 07';'Gage 08';'Gage 09';'Gage 10';...
    'Gage 11';'Gage 12';'Gage 13';'Gage 14';'Gage 15';'Gage 16'];
gagename2=[1:1:16];
gagename3=[1,1,2,2,3,3,4,4,5,5,6,6,7,7,8,8,9,9,10,10,11,11,12,12,13,13,...
    14,14,15,15,16,16];
numberofgage=16;
Vbridgesupply=input(1,7);%voltage supplied to wheatstone bridge
Patm_bar=input(1,8); %atmospheric pressure in bars
Patm=Patm_bar/6894.75;%convert to psi
r=0.892;%recovery factor for turbulent flow
Kelvin_con=273.15;%convert deg C to Kelvins
%name input data
for a=1:numberofgage
    k_l(a)=input(a,1); %k/l W/m^2-K
    Kcalib(a)=input(a,2);%TFG calibration slope ohm/C
    R20(a)=input(a,3);%TFG Resistance at 20 deg C
    x_c(a)=input(a,4);%x/c location of gage
    M_loc(a)=input(a,5);%local Mach number at gage location
    Rprun(a)=input(a,6);%pre-run resistance of TFG gage
end
%filter NI data
aba=size(NI_data_prefilt);%number of data columns
[d,e] = butter(5,30/500);%define filter
for i = 2:aba(2)%every NI column except time
    NI_data(:,i) = filtfilt(d,e,NI_data_prefilt(:,i));
end
%time data
time=NI_data_prefilt(:,1);
time=time-time(1);%convert b/c sometimes DAQ doesn't start time at zero
N=length(NI_data);
Npsi=length(PSI_data);
%name and sort NI data
for a=1:numberofgage
    %NI Column structure time, TFG backwalls,tfreetot,TFG voltages
    for b=1:N
        T_backwall(b,a)=NI_data(b,a+1);%deg C
        T_free_tot_prelag(b)=NI_data(b,2+numberofgage);%deg C
        TFG_volt(b,a)=NI_data(b,numberofgage+a+2);%Volt
        Ttot_plen_slide_NI(b)=NI_data(b,2*numberofgage+4);%sampled from
    end
end
%%%%%%%%%%%%name and sort initial value file%%%%%%%%%%%%%%%%%
for a=1:numberofgage
    %NI Column structure time, TFG backwalls,tfreetot,TFG voltages
    for b=1:length(init_data)
        T_backwall_initial(b,a)=init_data(b,a+1);%deg C
        TFG_volt_initial(b,a)=init_data(b,numberofgage+a+2);%volt
    end
end
for a=1:numberofgage
    T_TFG_init(a)=mean(T_backwall_initial(:,a));
    TFG_volt_init(a)=mean(TFG_volt_initial(:,a));
end
%%%%%%%%%%%%%%%%%%%%%%%%%%%%%%%%%%%%%%%%%%%%%%%%%%%%%%%%%%%%%%%%%%%%%%%%
lagTC=0.1;%lag the freestream TC measurement --located upstream
T_free_tot=zeros(1,N);
T_lag=T_free_tot_prelag(lagTC*fs:N);
for b=1:length(T_lag)
    T_free_tot(b)=T_free_tot(b)+T_lag(b);
end
%name PSI data (all data is in units of PSI)
ttpsi=0;
lead_psi=0.6;%seconds to lead psi data--psi trigger takes time to start
psi_count=psi_fs*lead_psi;
for c=1:Npsi
        Ptot_up(c)=PSI_data(psi_count,1);
        Pstat_free_up(c)=PSI_data(psi_count,2);
        Pstat_up_1(c)=PSI_data(psi_count,3);
        Pstat_up_2(c)=PSI_data(psi_count,4);
```

```
        Pstat_up_3(c)=PSI_data(psi_count,5);
        Pstat_down_1(c)=PSI_data(psi_count,6);
        Pstat_down_2(c)=PSI_data(psi_count,7);
        Pstat_down_3(c)=PSI_data(psi_count,8);
        Pstat_down_4(c)=PSI_data(psi_count,9);
        Orifice_up(c)=PSI_data(psi_count,10);
        Orifice_down(c)=PSI_data(psi_count,11);
        Orifice_up_Ptot(c)=PSI_data(psi_count,12);
        Orifice_up_Pstat(c)=PSI_data(psi_count,13);
        Ptot_plen(c)=PSI_data(psi_count,14);
        Pstat_plen(c)=PSI_data(psi_count,15);
        Pstat_down_avg(c)=(Pstat_down_1(c)+Pstat_down_2(c)+Pstat_down_3(c)...
            +Pstat_down_4(c))/4;
        Pr_up(c)=(Ptot_up(c)+Patm)/(Pstat_free_up(c)+Patm);
        Pr_down(c)=(Ptot_up(c)+Patm)/(Pstat_down_avg(c)+Patm);
        M_up(c)=sqrt(2/0.4*(Pr_up(c)^(.4/1.4)-1));
        M_down(c)=sqrt(2/0.4*(Pr_down(c)^(.4/1.4)-1));
        Orifice_dP(c)=Orifice_up(c)-Orifice_down(c);
        time_psi(c)=ttpsi;
        ttpsi=ttpsi+1/psi_fs;%make a time vector the same length as the psi data
        if psi_count<Npsi
            psi_count=psi_count+1;
        else
            psi_count=600;
        end
end
%%%%find tunnel start time
pp=1;
for n=1:Npsi;
    if Ptot_up(n)>0.007
        break
    end
    pp=pp+1;
end
tunnel_start_count=pp;
tunnel_start=pp/psi_fs;%tunnel start time in seconds
%for blowing calculations, must oversample data b/c NI samples MKS
%transducers at a very high rate
z=1;
for a=1:50:N
    Tfree_tot_blow(z)=T_free_tot(a);%tunnel tot
    Ttot_plen_fit(z)=NI_data(a,2*numberofgage+3);%Ttot plenum on fitting
    Ttot_plen_slide(z)=NI_data(a,2*numberofgage+4);%sliding plenum Ttot
    Orifice_up_Ttot(z)=NI_data(a,2*numberofgage+5);%Ttot line-upstream of orifice
    z=z+1;
end

A_holes=47*pi/4*(0.033*2.54/100)^2;%area of cooling holes m^2
discharge_coef=0.62;%discharge coefficient of orifice plate
bore_area=pi/4*(0.2795*2.54/100)^2;%m^2 area of orifice plate
%%%calculate blowing conditions
for a=1:Npsi
    Pr_plen(a)=(Ptot_plen(a)+Patm)/(Pstat_plen(a)+Patm);
    M_plen(a)=sqrt(2/0.4*(Pr_plen(a)^(.4/1.4)-1));
    Tstat_free(a)=(Tfree_tot_blow(a)+Kelvin_con)/(1+0.2*M_up(a)^2);%K
    Tstat_free_down(a)=(Tfree_tot_blow(a)+Kelvin_con)/(1+0.2*M_down(a)^2);%downstream
stat temp K
    rho_stat_free(a)=(Pstat_free_up(a)+Patm)*6894.75/(287*Tstat_free(a));%upstream
density kg/m^3

rho_stat_free_down(a)=(Pstat_down_avg(a)+Patm)*6894.75/(287*Tstat_free_down(a));%downstre
am density kg/m^3
    rhou_free(a)=rho_stat_free(a)*M_up(a)*sqrt(1.4*287*Tstat_free(a));%kg/m^2-s
    pr_orf_up(a)=(Orifice_up_Pstat(a)+Patm)/(Orifice_up_Ptot(a)+Patm);
    Tstat_line(a)=(Orifice_up_Ttot(a)+Kelvin_con)*pr_orf_up(a)^(0.4/1.4); %upstream of
orifice plate(K)
    rho_line(a)=(Orifice_up_Pstat(a)+Patm)*6894.75/(287*Tstat_line(a));
    mdot_cool(a)=discharge_coef*bore_area*sqrt(2*rho_line(a)*Orifice_dP(a)*6894.75);%kg/s
    Tstat_plen(a)=(Ttot_plen_slide(a)+Kelvin_con)/(1+0.2*M_plen(a)^2);%K --using Tprobe
slide into plenum
    rho_plen(a)=(Pstat_plen(a)+Patm)*6894.75/(287*Tstat_plen(a));%kg/m^2
```

```
    mu(a)=0.00001716*((Tfree_tot_blow(a)+Kelvin_con)/273.16)^1.5*...
        (383.716/((Tfree_tot_blow(a)+Kelvin_con)+110.556));
    vel_down(a)=M_down(a)*sqrt(1.4*287*Tstat_free_down(a));
    Re_down(a)=rho_stat_free_down(a)*vel_down(a)*(2.7505*2.54/100)/mu(a);
    DR(a)=rho_plen(a)/rho_stat_free(a);%Density Ratio
    PR(a)=(Ptot_plen(a)+Patm)/(Ptot_up(a)+Patm);%Pressure Ratio
    BR(a)=(mdot_cool(a)/A_holes)/rhou_free(a);%Blowing Ratio
end
  clear NI_data NI_data_prefilt PSI_data

M_down_t=M_down';%transpose matrix for saving
time_psi_t=time_psi';
%%%%HTC Data reduction
HTC_reduce_time=3;
reducestart=tunnel_start+3;
reduceend=reducestart+HTC_reduce_time;
%draw lines to show where reducing data starts and ends
red_start_x=[reducestart,reducestart];
red_end_x=[reduceend,reduceend];
red_start_y=[0,40e3];
red_end_y=[0,40e3];
Mach_redtime=M_down(1,round(reducestart*psi_fs):round(reduceend*psi_fs));
BR_redtime=BR(1,round(reducestart*psi_fs):round(reduceend*psi_fs));
DR_redtime=DR(1,round(reducestart*psi_fs):round(reduceend*psi_fs));
Re_redtime=Re_down(1,round(reducestart*psi_fs):round(reduceend*psi_fs));
Mex_avg=mean(Mach_redtime);
BR_avg=mean(BR_redtime);
DR_avg=mean(DR_redtime);
Re_avg=mean(Re_redtime);
Mstring=['Mex= ' num2str(Mex_avg)];
BRstring=['BR= ' num2str(BR_avg)];
DRstring=['DR= ' num2str(DR_avg)];
%Plot Mach Number and BR--shows data reduction window
figure
hold on
title(Rund)
hl1=line(time_psi,M_down,'Color','b');
axis([tunnel_start 30 0 1.1])
xlabel('Time,(s)')
ylabel('Mach, Exit')
line(red_start_x,red_start_y)
line(red_end_x,red_end_y)
ax1=gca;
set(ax1,'XColor','b','Ycolor','b')
ax2=axes('Position',get(ax1,'Position'),'YAxisLocation',...
    'right','Color','none','XColor','k','YColor','k');
hl2=line(time_psi,BR,'Color','k','Parent',ax2);
axis([tunnel_start 30 0 2])
ylabel('Blowing Ratio')
text(20,0.5,{Mstring,BRstring,DRstring},'EdgeColor','black')
hold off
savedata=0
%%%%%%%%%%%%%%%%Convert TFG voltages to temperature
Rline=0.145;%resistance of cord
Rs=10000;%series resistance of bridge
for a=1:numberofgage
    TFG_volt(:,a)=TFG_volt(:,a)-TFG_volt_init(a);%offset TFG voltage to zero
    %correct the calibration for day to day variation
    Kcor(a)=Kcalib(a)*(Rprun(a)-Rline)/R20(a);
    Rt(a)=Rline+Rs+Rprun(a);
    for j=1:N
        del_T_Pt_TFG(j,a)=TFG_volt(j,a)*Rt(a)/(Kcor(a)*...
            (Rs/Rt(a)*Vbridgesupply-TFG_volt(j,a)));
        T_Pt_TFG(j,a)=T_TFG_init(a)+del_T_Pt_TFG(j,a);%deg C
        %TFG finds change in temp, so must add initial temp
        q_to_blade(j,a)=k_l(a)*(T_Pt_TFG(j,a)-T_backwall(j,a));
        %local Taw for uncooled (Kelvins)
        Trec(j,a)=(T_free_tot(j)+Kelvin_con)*...
            ((1+r*0.2*M_loc(a)^2)/(1+.2*M_loc(a)^2));
    end
end
```

```
%%%%%%%%%%%%%%%calculations of h and eta
for a=1:numberofgage
    ggg=1;
%reduce HTC for set time after  tunnel start
    for j=round(reducestart*fs):round(reduceend*fs)
        yax(ggg,a)=q_to_blade(j,a)/...
            (Trec(j,a)-(Ttot_plen_slide_NI(j)+Kelvin_con));
        xax(ggg,a)=(Trec(j,a)-(T_Pt_TFG(j,a)+Kelvin_con))...
            /(Trec(j,a)-(Ttot_plen_slide_NI(j)+Kelvin_con));
        ggg=1+ggg;
    end
    lineeq_o=polyfit(xax(:,a),yax(:,a),1);
    lineeq(1,a)=lineeq_o(1);
    lineeq(2,a)=lineeq_o(2);
    R_coef=corrcoef(xax(:,a),yax(:,a));
    R_squared(1,a)=R_coef(2,1)^2;
    evallinex(:,a)=(linspace((min(xax(:,a))-0.01),(max(xax(:,a))+0.01),10))';
    evalliney(:,a)=(lineeq(1,a)*evallinex(:,a)+lineeq(2,a));
    eta(1,a)=-lineeq(2,a)/lineeq(1,a);
    HTC_avg(1,a)=lineeq(1,a);
end
xtextloc=1.04*mean(xax);
ytextloc=0.96*mean(yax);
%%%reduce HTC and Taw time history--assuming eta is constant for entire run
%%%should only analyze results during time eta is calculated from.
for a=1:numberofgage
    for b=1:N
        %Taw (K)  --assuming eta=k for run
        Taw(b,a)=eta(1,a)*...
            (Ttot_plen_slide_NI(b)+Kelvin_con-Trec(b,a))+Trec(b,a);
        %HTC time history W/m^2-K
        HTC(b,a)=q_to_blade(b,a)/(Taw(b,a)-(T_Pt_TFG(b,a)+Kelvin_con));
    end
end
%%%%%%%%%%%%%SAVE OUTPUT%%%%%%%%%%%%%%%%%%%%%%%%%%%%
%stop reduction and look at conditions to see if you want to save the data
%check out reduction window and see if flow conditions are steady
%if you choose, data will be saved in an excel file organized into
%separate tabs of data
keyboard

if savedata==1
    Nu_avg=HTC_avg*(2.7505*2.54/100)/0.03;
    oddcount=1;
    evencount=2;
    for a=1:numberofgage
        axisdata(:,oddcount)=xax(:,a);
        axisdata(:,evencount)=yax(:,a);
        oddcount=oddcount+2;
        evencount=evencount+2;
    end
    xlswrite(savename,gagename3,'Average Values','B1')
    xlswrite(savename,axisdata,'axisdata','B2')
    avgarray(1,:)=HTC_avg(1,:);
    avgarray(2,:)=eta(1,:);
    avgarray(3,:)=R_squared(1,:);
    avgarray(5,1)=Mex_avg;
    avgarray(6,1)=BR_avg;
    avgarray(7,1)=DR_avg;
    avgarray(9,1)=reducestart;
    avgarray(10,1)=reduceend;
    avgarray(12,1)=tunnel_start;
    avgarray(14,:)=T_TFG_init(1,:);
    avgarray(15,:)=TFG_volt_init(1,:);
    avgarray(17,:)=Nu_avg(1,:);
    avgarray(18,1)=Re_avg;
    xlswrite(savename,gagename2,'Average Values','B1')
    xlswrite(savename,avgarray,'Average Values','B2')

    savearray_flow(:,1)=time_psi_t;
    savearray_flow(:,2)=M_down_t;
```

```
    savearray_flow(:,3)=Ptot_up';
    savearray_flow(:,4)=Pstat_free_up';
    savearray_flow(:,5)=Pstat_up_1';
    savearray_flow(:,6)=Pstat_up_2';
    savearray_flow(:,7)=Pstat_up_3';
    savearray_flow(:,8)=Pstat_down_1';
    savearray_flow(:,9)=Pstat_down_2';
    savearray_flow(:,10)=Pstat_down_3';
    savearray_flow(:,11)=Pstat_down_4';
    savearray_flow(:,12)=Tfree_tot_blow';

    xlswrite(savename,savearray_flow,'Flow History','A2')
    T_free_tot_s=T_free_tot(1,1:N);
    T_free_tot=T_free_tot';
    savearray_blowing(:,1)=time_psi_t(:,1);
    savearray_blowing(:,2)=BR';
    savearray_blowing(:,3)=DR';
    savearray_blowing(:,4)=PR';
    savearray_blowing(:,5)=M_plen';
    savearray_blowing(:,6)=Tstat_free';
    savearray_blowing(:,7)=rho_stat_free';
    savearray_blowing(:,8)=mdot_cool';
    savearray_blowing(:,9)=Tstat_plen';
    savearray_blowing(:,10)=Ptot_plen';
    savearray_blowing(:,11)=Pstat_plen';
    savearray_blowing(:,12)=Ttot_plen_fit';
    savearray_blowing(:,13)=Ttot_plen_slide';
    xlswrite(savename,savearray_blowing,'Blowing','A2')
    %oversample data to save
    time_s=time(1:10:N,1);
    for a=1:numberofgage
        yyy=1;
        for zzz=1:10:N
            T_backwall_s(yyy,a)=T_backwall(zzz,a);
            T_Pt_TFG_s(yyy,a)=T_Pt_TFG(zzz,a);
            HTC_s(yyy,a)=HTC(zzz,a);
            q_to_blade_s(yyy,a)=q_to_blade(zzz,a);
            Taw_s(yyy,a)=Taw(zzz,a);
            Trec_s(yyy,a)=Trec(zzz,a);
            Tcool_s(yyy)=Ttot_plen_slide_NI(zzz);
            yyy=1+yyy;
        end
    end
    %heat flux data
    xlswrite(savename,gagename2,'Tbackwall','B1')
    xlswrite(savename,T_backwall_s,'Tbackwall','B2')
    xlswrite(savename,gagename2,'T Pt TFG','B1')
    xlswrite(savename,T_Pt_TFG_s,'T Pt TFG','B2')
    xlswrite(savename,gagename2,'HTC','B1')
    xlswrite(savename,HTC_s,'HTC','B2')
    xlswrite(savename,gagename2,'Heat Flux','B1')
    xlswrite(savename,q_to_blade_s,'Heat Flux','B2')
    xlswrite(savename,gagename2,'Taw','B1')
    xlswrite(savename,Taw_s,'Taw','B2')
    xlswrite(savename,gagename2,'Trec','B1')
    xlswrite(savename,Trec_s,'Trec','B2')
    xlswrite(savename,T_free_tot_s','Ttot free','B2')
    xlswrite(savename,Tcool_s','Tcool','B2')
end
tunnel_run_time=tunnel_start:psi_fs:30;
%%%%%%%%%%%%%%%%%%%%PLOTS%%%%%%%%%%%%%%%%%%%%
figure
plot(x_c,HTC_avg,'o')
xlabel('x/c')
ylabel('HTC, (W/m^2-K)')
figure
plot(x_c,eta,'o')
xlabel('x/c')
ylabel('\eta')
figure
plot(x_c,del_q_r,'o')
```

```
xlabel('x/c')
ylabel('\Delta''q_r, (W/m^2)')
%Plot Mach Number and DR
figure
hold on
title(Rund)
hl1=line(time_psi,M_down,'Color','b');
axis([tunnel_start 30 0 1])
xlabel('Time,(s)')
ylabel('Mach, Exit')
line(red_start_x,red_start_y)
line(red_end_x,red_end_y)
ax1=gca;
set(ax1,'XColor','b','Ycolor','b')
ax2=axes('Position',get(ax1,'Position'),'YAxisLocation',...
    'right','Color','none','XColor','k','YColor','k');
hl2=line(time_psi,DR,'Color','k','Parent',ax2);
axis([tunnel_start 30 0 2])
ylabel('Density Ratio')
text(20,1,{Mstring,BRstring,DRstring},'EdgeColor','black')
hold off
%Mach
figure
hold on
xlabel('Time (s)')
line(red_start_x,red_start_y)
line(red_end_x,red_end_y)
ylabel('Mexit')
axis([tunnel_start,30,0,1])
plot(time_psi,M_down)
hold off
% BR
figure
hold on
xlabel('Time (s)')
% ylabel('Blowing Ratio')
line(red_start_x,red_start_y)
line(red_end_x,red_end_y)
% axis([tunnel_start,30,0,3])
% plot(time_psi,BR)
hold off
% PR
figure
hold on
xlabel('Time (s)')
ylabel('Pressure Ratio')
line(red_start_x,red_start_y)
line(red_end_x,red_end_y)
axis([tunnel_start,30,0,2])
plot(time_psi,PR)
hold off
% DR
figure
hold on
xlabel('Time (s)')
ylabel('Density Ratio')
axis([tunnel_start,30,0,3])
line(red_start_x,red_start_y)
line(red_end_x,red_end_y)
% plot(time_psi,DR)
hold off
%temperature plots
figure
hold on
title({Rund})
axis([0 30 200 400])
plot(time,(T_free_tot+Kelvin_con),time,...
    Taw(:,a),time,Trec(:,a),time,(Ttot_plen_slide_NI+Kelvin_con))
legend('Ttot free','Taw','Trec','Tcoolant')
line(red_start_x,red_start_y)
line(red_end_x,red_end_y)
```

```
xlabel('Time (s)')
ylabel('Temperature (K)')

hold off
%%%%%%%%%%%%%%subplots of all gage signals%%%%%%%%%%%%%%%
figure
for a=1:numberofgage/2
    subplot(4,2,a);plot(time,T_Pt_TFG(:,a),time,T_backwall(:,a))
    xlabel('Time (s)')
    ylabel('T,(C)')
    title(gagename(a,:))

end

figure
for a=numberofgage/2+1:numberofgage
    subplot(4,2,a-8);plot(time,T_Pt_TFG(:,a),time,T_backwall(:,a))
    xlabel('Time (s)')
    ylabel('T,(C)')
    title(gagename(a,:))

end

figure
for a=1:numberofgage/2
    subplot(4,2,a);plot(time,(T_Pt_TFG(:,a)-T_backwall(:,a)))
    xlabel('Time (s)')
    ylabel('\Delta T')
    title(gagename(a,:))

end

figure
for a=numberofgage/2+1:numberofgage
    subplot(4,2,a-8);plot(time,(T_Pt_TFG(:,a)-T_backwall(:,a)))
    xlabel('Time (s)')
    ylabel('\Delta T')
    title(gagename(a,:))

end

figure
for a=1:numberofgage/2
    subplot(4,2,a);plot(time,HTC(:,a))
    line(red_start_x,red_start_y)
    line(red_end_x,red_end_y)
    axis([0 20 0 1000])
    xlabel('Time (s)')
    ylabel('h')
    title(gagename(a,:))

end

figure
for a=numberofgage/2+1:numberofgage
    subplot(4,2,a-8);plot(time,HTC(:,a))
    line(red_start_x,red_start_y)
    line(red_end_x,red_end_y)
    axis([0 20 0 1000])
    xlabel('Time (s)')
    ylabel('h')
    title(gagename(a,:))

end

%%%%plots of data reduction line fit method
for a=1:numberofgage
    hstring=['h= ' num2str(round(lineeq(1,a))) ' W/m^2-K'];
    etastring=['\eta= ' num2str(eta(1,a))];
    regstring=['R^2= ' num2str(R_squared(1,a))];
    figure
```

```
    hold on
    title({Rund,gagename(a,:)})
    xlabel('(Tr-Tw)/(Tr-Tc)')
    ylabel('q/(Tr-Tc)')
    plot(xax(:,a),yax(:,a),'.','MarkerSize',4)
    plot(evallinex(:,a),evalliney(:,a),'-k')
    text(xtextloc(a),ytextloc(a),...
        {hstring,etastring,regstring},'EdgeColor','black')
    hold off
    slope(1,a)=lineeq(1,a);
    yint(1,a)=lineeq(2,a);
end

figure
for a=1:numberofgage/2
    subplot(4,2,a);plot(time,TFG_volt(:,a))
    xlabel('Time (s)')
    ylabel('Volt')
    title(gagename(a,:))
end

figure
for a=numberofgage/2+1:numberofgage
    subplot(4,2,a-8);plot(time,TFG_volt(:,a))
    xlabel('Time (s)')
    ylabel('Volt')
    title(gagename(a,:))
end

figure
for a=1:numberofgage/2
    subplot(4,2,a);plot(time,phi(:,a))
    xlabel('Time (s)')
    ylabel('\phi')
    title(gagename(a,:))
    axis([reducestart reduceend 0 1])
end

figure
for a=numberofgage/2+1:numberofgage
    subplot(4,2,a-8);plot(time,phi(:,a))
    xlabel('Time (s)')
    ylabel('\phi')
    title(gagename(a,:))
    axis([reducestart reduceend 0 1])
end

figure
for a=1:numberofgage/2
    subplot(4,2,a);
    plot(time,q_to_blade(:,a),time,q_FD_backwall(:,a),time,q_FD_TFG(:,a))
    xlabel('Time (s)')
    ylabel('q,W/m^2')
    title(gagename(a,:))
    axis([0 30 0 25e3])
    legend('DS','T_B','T TFG')
end

figure
for a=numberofgage/2+1:numberofgage
    subplot(4,2,a-8);
    plot(time,q_to_blade(:,a),time,q_FD_backwall(:,a),time,q_FD_TFG(:,a))
    xlabel('Time (s)')
    ylabel('q,W/m^2')
    title(gagename(a,:))
    axis([0 30 0 25e3])
    legend('DS','T_B','T TFG')
end
fprintf('done')
```

Appendix G: Reasons for Gage Failure

The film cooling performance of this airfoil and cooling configuration has been characterized in the showerhead region. However, the double-sided heat flux gage implemented in this work provided a gage yield that is unacceptable for use in future experiments. Sixteen gages were instrumented over the surface of the blade; of these, only five generated data that was repeatable and explainable within the trends described in literature.

The causes of gage failure stem from:

- platinum thin film gage durability
- contact resistance between the backwall thermocouple and blade material
- installation difficulties

An example of platinum thin film gage erosion can be seen in Figure G-1. The platinum thin film gage is constructed of a platinum wire connected to a copper lead. To secure the electrical connection of the platinum wire, copper is layered both above and below the platinum. In this testing, several gages showed erosion. Many of the platinum thin film gages that showed this erosion problem provided voltage signals that did not match the general trend of signals seen by other thin film gages. It is possible that adding the thermocouple below the gage added more stress to the gage material causing its erosion.

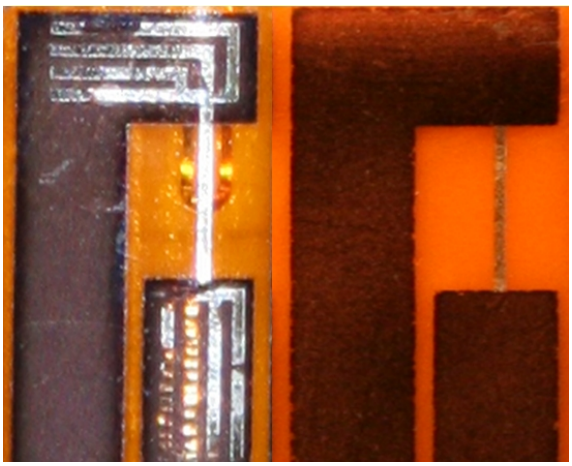

Figure G-1. Illustration of gage erosion. The gage on the left is a double-sided gage that shows exposed platinum connection to leads. The gage on the right is an example of a single-sided gage that has been through testing without erosion.

Contact resistance between the thermocouple and macor substrate is another suspected problem with this gage configuration. The contact resistance is difficult to characterize because of its inherent variability. Every attempt was made to provide for consistent gage construction and installation. However, because of the wide ranging thermal conditions subjected on the instrumentation, thermal stresses could have caused the contact resistance to change with time. It was hoped that during the gage installation that since the adhesive layer was thicker than the thermocouple that the adhesive would fill any voids between the gage and blade surface. While no air bubbles can be seen from physical inspection, it is possible that air gaps cause a changing contact resistance. The variable temperature and pressure exerted by the wind tunnel create an environment where the adhesive layer could fail or vary in effectiveness yielding inconsistent gage installation.

The gage installation procedure described in Appendix B was a tedious and time consuming process. There were a total of 64 lead wires that had to be soldered to the gages over the small confinements of the blade surface. With a construction and installation procedure this tedious, inconsistencies are bound to occur.

Because a lower spatial resolution measurement of Nusselt number and film cooling effectiveness was achieved than was the goal of this study, ideas for future improvement are provided in Appendix H.

Appendix H: Future Work

The second phase of this project is to study the film cooling performance over the surface of a film cooled vane. This appendix presents two ideas for an improved measurement technique on the vane. If either of these techniques are successful on the vane, experiments could be redone on the blade to provide for better spatial resolution and a greater measurement extent. The key to these experiments is measuring the heat flux, so two techniques are presented for this type of measurement. The first technique is to use a single sided gage in the film cooled environment by reducing the density ratio of the tests, and the second technique is to use a double-sided gage like that described by Ewing [C-1].

Single Sided Gage

The reason for implementing a double-sided thin film gage was that when matching the density ratio with that of engine representative conditions, the cooling air must be at such a low temperature that it causes conduction around the plenum region to become two-dimensional. This two dimensional conduction invalidates the assumptions used when implementing a single sided gage such as that used by Carullo *et al*.[17] If, instead of matching the density ratio of an engine, coolant air can be provided at the same temperature as the initial core temperature of the blade, one dimensional heat flux can be assumed.

This cooling configuration can be imposed by heating the air supplied to the blade to the core temperature of the blade. The core temperature of the blade stays constant over the course of a tunnel run, but can increase over the course of a day. The core temperature of the blade generally ranges from 22º C to 29º C over a day of heated tunnel runs. Preliminary experiments have shown that coolant air can be supplied at this range of temperatures by passing the coolant supply through a coil of pipe immersed in a hot water bath. The corresponding density ratio would be DR=1.4. The density ratio has a secondary impact on the effect of film cooling, Bogard and Thole [2], so an experiment under these conditions would be able to successfully characterize the cooling performance over this blade.

The next portion of this project will be testing on a film cooled vane. A two-dimensional, finite element model of the vane at the conditions proposed is provided in

Figure H-1. External boundary conditions are the heat transfer coefficient augmentation predicted from this study combined with results from Nasir *et al.*[H-1] and the total temperature during a typical tunnel run. The initial temperature of the blade core and coolant temperature are matched. It appears from this simulation that a one-dimensional conduction profile can be assumed and that a single sided gage can be used when reducing the desired coolant to freestream density ratio.

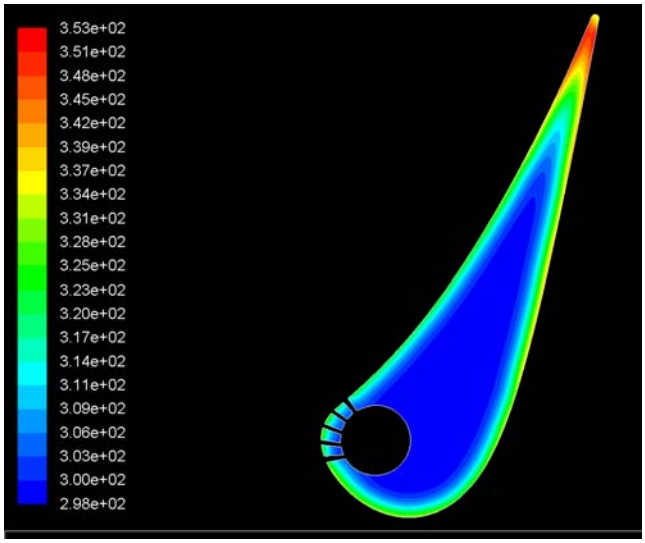

Figure H-1. Temperature profile of a film cooled vane. The coolant temperature is at the same temperature as the initial core temperature of the vane.

Double-sided Gage

A thin, double-sided heat flux gage like that described by Ewing *et al.*[C-1] could be used to measure the heat flux into the blade. The same density ratio could be kept at an engine representative value because a one dimensional assumption only has to be made through the gage and not in the blade material. An advantage to this type of gage is that it can be manufactured in-house and therefore many types of gage arrangements can be made. This would allow for the measurement of spanwise variations in film cooling performance. Platinum thin film gages such as those implemented in this study must be individually calibrated and day to day variation of resistance must be accounted for. An advantage of the type of gage is that once material property calibration is documented, no further calibration is necessary.

With any double-sided gage, the material property calibration is of highest concern. The material property calibration can cause a high level of uncertainty in the

heat flux measurement leading directly to high uncertainty levels in heat transfer coefficient and film cooling effectiveness. If the material properties can be calibrated for at an acceptable level of uncertainty and a method for mounting the gages to the blade surface can be found, this type of double-sided gage would be a good option for heat flux measurement. The double-sided gage configuration is still in development by Diller at the time of this writing.

Appendix I: Sample Data

This appendix presents sample data for the calculation of heat transfer coefficient and film cooling effectiveness for one gage under the freestream conditions of M_e=0.78 and a BR=1.0. Results are presented for Gage 16, the gage located farthest downstream on the pressure side of the blade. An illustration of the tunnel freestream conditions is provided in Figure I-1. Mach number, density ratio, and blowing ratio are constant for a test run while the tunnel total temperature is constantly dropping. The transient nature and of the temperature and quasi-steady state conditions of the flow allow for the calculation of heat transfer coefficient and film cooling effectiveness during one run. Data reduction was done during a three second window where the flow conditions were quasi-steady and the heat flux signal was high providing for a large difference in temperature across the gage.

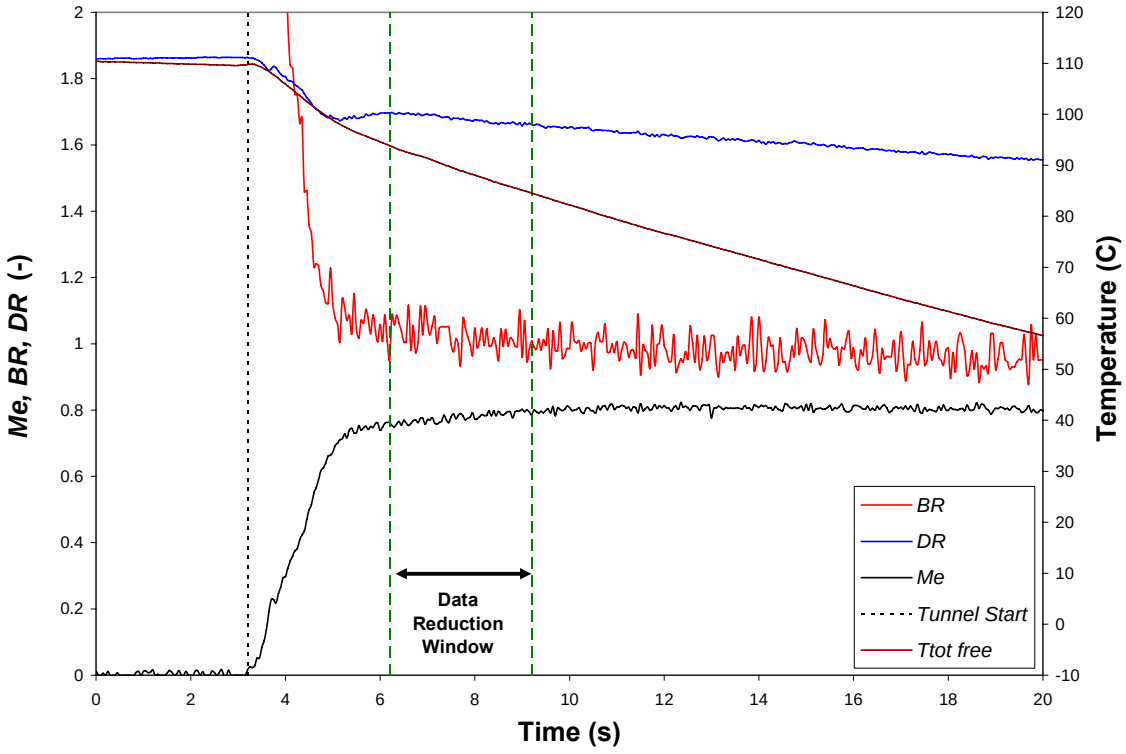

Figure I-1. Tunnel flow conditions. The exit Mach number, blowing ratio, and density ratio are plotted on the left axis while the tunnel total temperature is plotted on the right axis.

The temperature of the thermocouples and voltage of the platinum thin film gages are recorded by the National Instruments AT-MIO-16XE-50 (NI) system. The platinum

thin film gages are a resistance temperature device. The resistance versus temperature relationship of the TFG's are calibrated prior to testing using the procedure outlined by Cress [20]. A wheatstone bridge circuit is used to measure the changing resistance of the gages in terms of voltage. The data reduction procedure outlined by Cress [20] is used to transform this voltage into temperature. The initial temperature of the gage is determined from the backwall thermocouple before the experiment when the blade is at a constant temperature. The temperature of the backwall thermocouples is measured with the NI system using internal cold junction compensation. A plot of the thin film gage and backwall thermocouple temperatures is provided in Figure I-2.

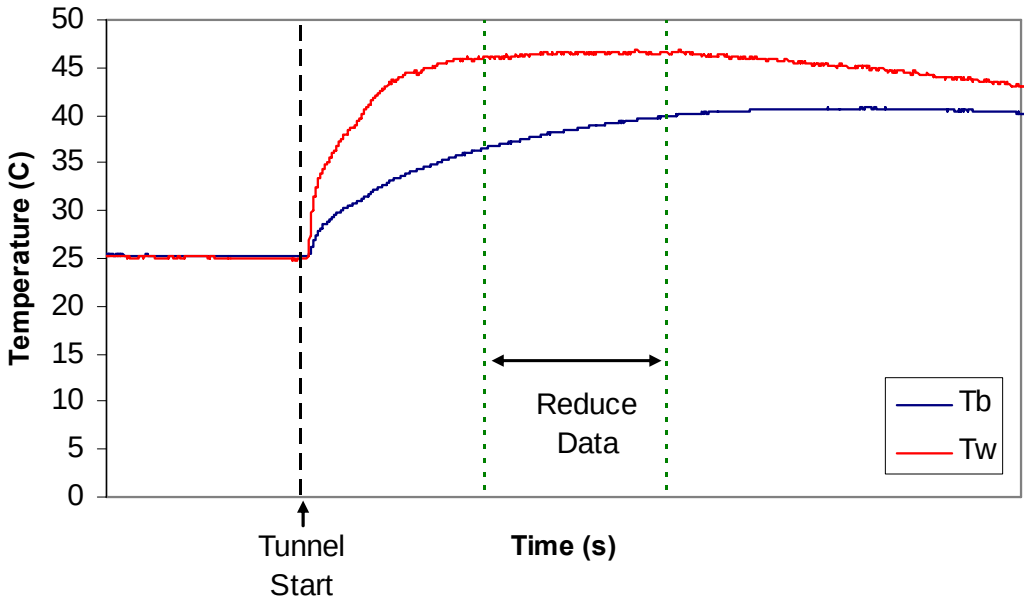

Figure I-2. Thin film gage and backwall thermocouple temperatures.

The temperature difference across the gage was calculated and multiplied by the *k/l* value of 1240 W/m^2-K. This is described in Equation 3, and provides for the heat flux through the gage. The temperature difference across the gage and the associated heat flux is shown in Figure I-3. Once the heat flux had been calculated, the heat transfer coefficient could be determined from plotting Equation 7. A sample of this plotting is shown in Figure I-4.

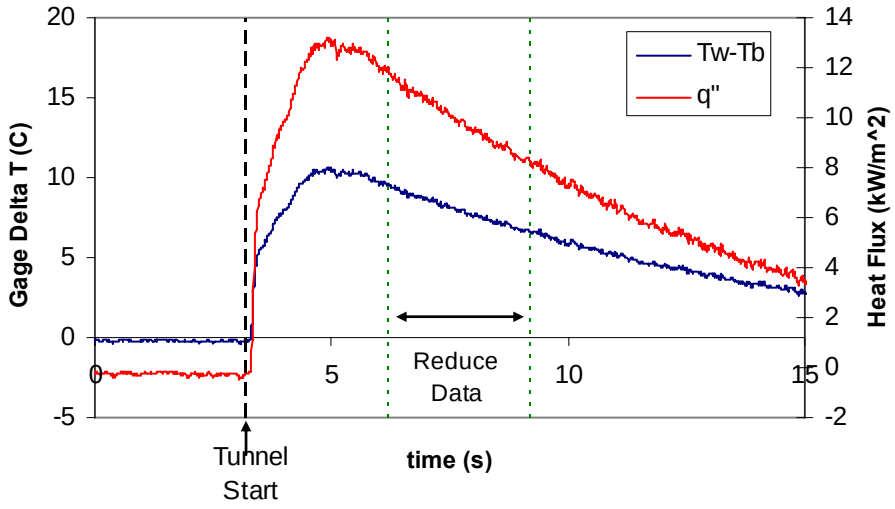

Figure I-3. Temperature difference across the gage and the corresponding heat flux.

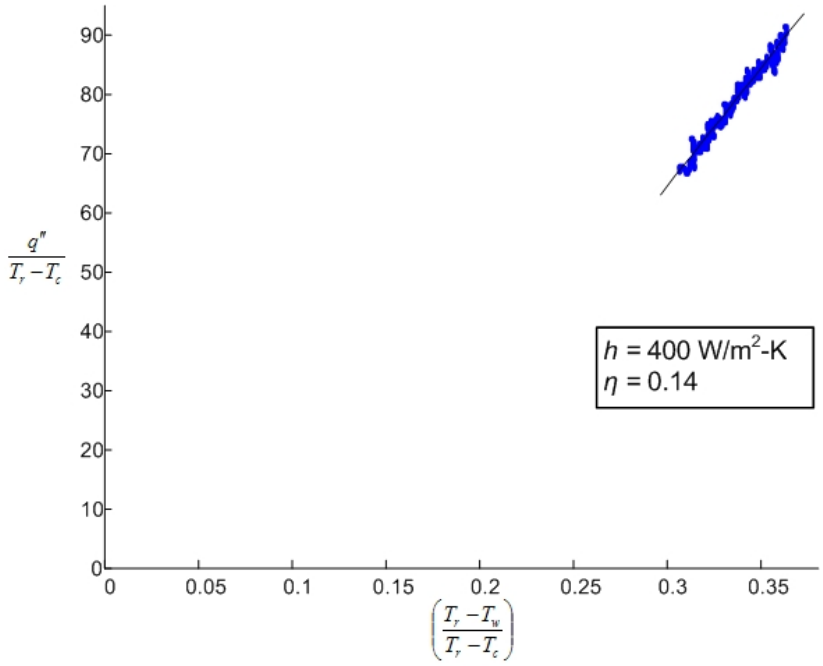

Figure I-4. Transient procedure for finding h and η.

From the effectiveness data determined through the line fit procedure shown in Figure I-4. The adiabatic wall temperature could be solved. The adiabatic wall temperature could be used to plot a time history of the heat transfer coefficient. This time history is provided in Figure I-5. The value of the time history heat transfer coefficient

plotted in Figure I-5 and the average value provided by the line fitting scheme shown in Figure I-4 match.

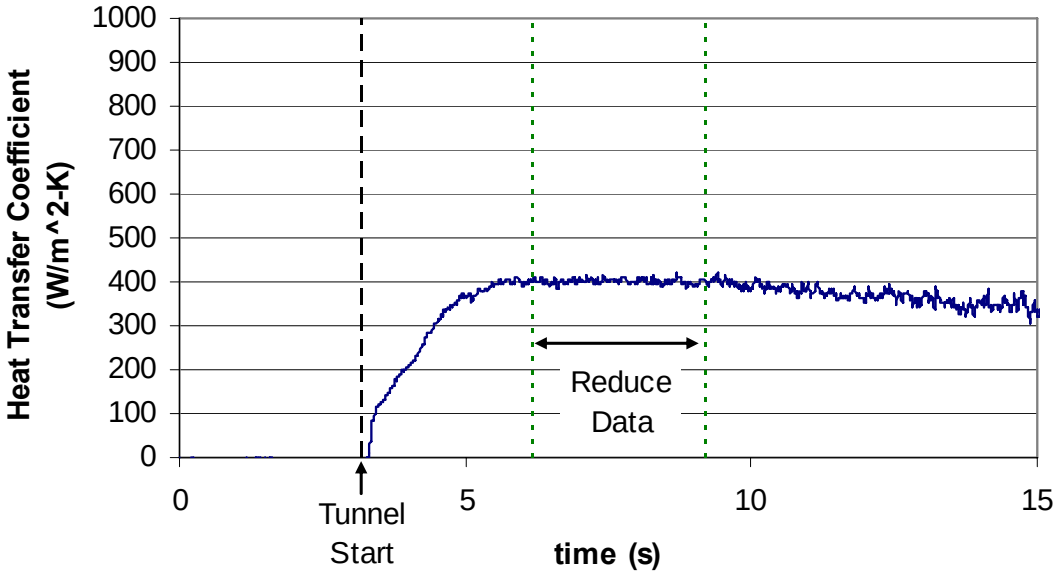

Figure I-5. Time history of heat transfer coefficient.

Vita

Ashley Ray Guy was born December 20, 1982 and raised in Union, West Virginia. He graduated from James Monroe High School in 2001 as a National Merit Scholar and president of the student body. Ash attended Virginia Tech from 2001 to 2006 where he graduated with his Bachelor's of Science in Mechanical Engineering, Summa Cum Laude in May 2006. While attending Virginia Tech he co-oped at Honeywell Aerospace in Greer, SC for three semesters and studied abroad at Technische Universität Darmstadt, Germany for one semester. Ash worked as an undergraduate research assistant under the direction of Dr. Wing Ng in the field of gas turbine aerodynamics. Subsequent to graduation with his bachelor's degree, he was awarded the Aerojet Propulsion Fellowship and accepted a position as a graduate research assistant under Dr. Ng. Ash conducted research in gas turbine compressor aerodynamics, turbine aerodynamics, and turbine heat transfer with funding provided by General Electric, Rolls-Royce, and Solar Turbines, respectively. Ash graduated with his Master's of Science degree in Mechanical Engineering in Summer 2007 and will begin a position in Fall 2007 as a machinery engineer for the ExxonMobil Development Corporation in Houston, Texas.